Direct calculation of interface warping functions for considering longitudinal discontinuities in beams

Dong-Hwa Lee, Hyo-Jin Kim and Phill-Seung Lee*

*Department of Mechanical Engineering, Korea Advanced Institute of Science and Technology,
291 Daehak-ro, Yuseong-gu, Daejeon 34141, Republic of Korea*

Abstract. In this paper, we present a new method to calculate interface warping functions for the analysis of beams with geometric and material discontinuities in the longitudinal direction. The classical Saint Venant torsion theory is extended to a three-dimensional domain by considering the longitudinal direction. The interface warping is calculated by considering both adjacent cross-sections of a given interface. We also propose a finite element procedure to simultaneously calculate the interface warping function and the corresponding twisting center. The calculated interface warping functions are employed in the continuum-mechanics based beam formulation to analyze arbitrary shape cross-section beams with longitudinal discontinuities. Compared to the previous work by Yoon and Lee (2014a), both geometric and material discontinuities are considered with fewer degrees of freedom and higher accuracy in beam finite element analysis. Through various numerical examples, the effectiveness of the proposed interface warping function is demonstrated.

Keywords: beams; continuum-mechanics based beam; finite element method; longitudinal discontinuity; torsion; warping

1. Introduction

Beam structures not only exist in nature, but have been widely used in many fields of engineering such as mechanical, marine, civil, and aerospace engineering. After the advent of the finite element method (FEM), FEM has been mainly used for the analysis of beam structures (Yoon and Lee 2014a, Batoz and Dhatt 1990, Vlasov 1961, Timoshenko and Goodier 1970, Gjelsvik 1981, Hughes 2000, Bathe 1996, Kim *et al*. 2020, Kim *et al*. 2021, Dvorkin *et al*. 1989, Pacoste and Eriksson 1997, Ibrahimbegović 1995, Ibrahimbegović 1997, Lee and McClure 2006, Cardona and Geradin 1988). It is well known that warping must be considered to accurately predict three-dimensional (3D) bending, stretching, and twisting behaviors and their couplings in beams (Gruttmann *et al*. 1999, Wagner and Gruttmann 2001, Wagner and Gruttmann 2002, Iesan 2008). The development of 3D beam finite elements that consider warping has long been an important research topic (Benscoter 1954, Yoon *et al*. 2012, Yoon and Lee 2014b, Yoon *et al*. 2015, Yoon *et al*. 2017a, b, El Fatmi 2007a, b, El Fatmi and Ghazouani 2011a, b, Sapountzakis and Mokos 2003, Sapountzakis and Mokos 2004, Petrov and Géradin 1998a, b, Genoese *et al*. 2013, Genoese *et al*. 2014, Mancusi and Feo 2013, Qureshi and Ganga 2014, Barretta *et al*. 2015, Pi and Bradford 2005, GonÇalves *et al*. 2010, Carrera *et al*. 2010, Battini and Pacoste 2002, Alsafadie *et al*. 2011).

To consider the warping effect accurately, it is essential to obtain an appropriate warping function for a given beam cross-section. The well-known Saint Venant torsion theory (Batoz and Dhatt 1990, Iesan 2008) has been employed to calculate free warping functions, which are frequently used as basis functions to represent the entire warping displacement field along with warping degrees of freedom (DOFs) in beam finite element analysis (Benscoter 1954, Yoon *et al*. 2012, Yoon and Lee 2014b, Yoon *et al*. 2015, Yoon *et al*. 2017a, b, El Fatmi 2007a, b, El Fatmi and Ghazouani 2011a, b, Sapountzakis and Mokos 2003, Sapountzakis and Mokos 2004). Then, general twisting kinematics can be formulated under various geometries, boundary conditions and loadings (Yoon and Lee 2014a, Yoon *et al*. 2012). Linear and nonlinear analysis is also available for composite cross-sections (Petrov and Géradin 1998a, b, Genoese *et al*. 2013, Genoese *et al*. 2014, Mancusi and Feo 2013, Qureshi and Ganga 2014, Barretta *et al*. 2015, Pi and Bradford 2005, GonÇalves *et al*. 2010, Carrera *et al*. 2010, Battini and Pacoste 2002, Alsafadie *et al*. 2011).

Most existing studies have focused on beams with constant or continuously varying cross-sections. Recently, Yoon and Lee (2014a) proposed a method to model warping displacement fields of discontinuously varying arbitrary cross-section beams. Adopting Lagrangian multipliers, the study introduced the calculation of interface warping functions to model warping at an interface where longitudinal geometric discontinuity occurs. However, since the interface warping functions are not complete by themselves, two free warping functions calculated from adjacent cross-sections of the given interface need to be additionally utilized along with degrees of freedom. This

*Corresponding author, Professor
 E-mail: phillseung@kaist.edu

(a) Cross-sections ① and ②, and the interface cross-section between them

(b) Free warping functions of cross-sections ① and ②, and the interface warping function at the interface cross-section
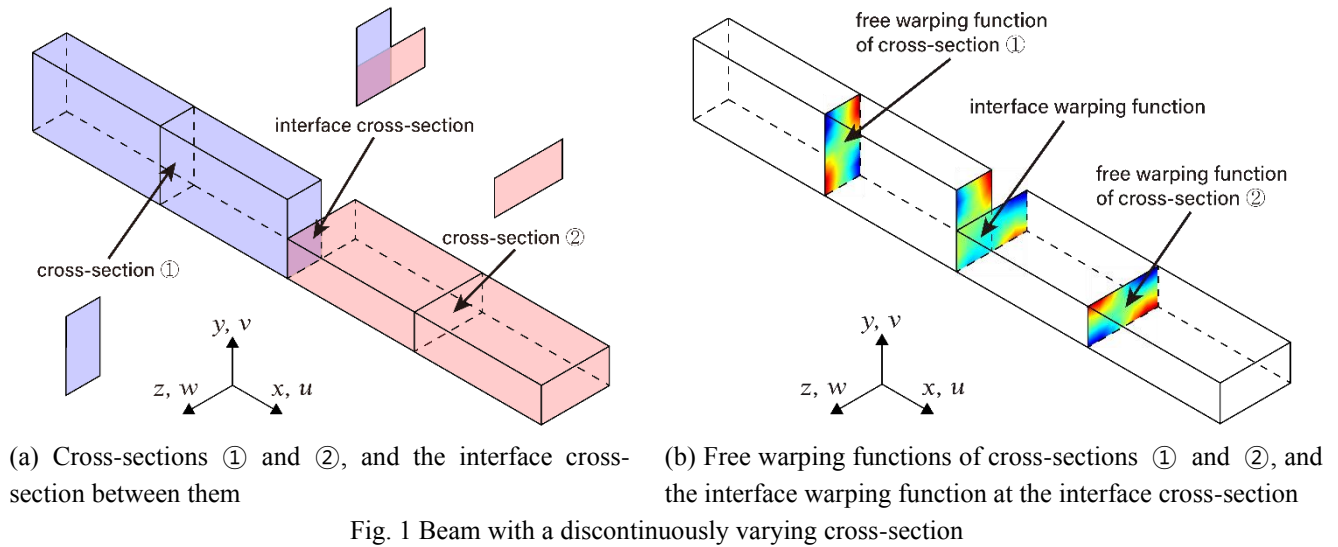
Fig. 1 Beam with a discontinuously varying cross-section

complexity makes it difficult to extend the numerical procedure for nonlinear analysis.

In this study, we develop a new formulation for calculating interface warping functions for beams with geometric and material discontinuities in the longitudinal direction. To represent the sudden change of twisting at an interface cross-section where discontinuity occurs, an interface warping function should be obtained considering both adjacent cross-sectional geometries and material properties. We extend the classical Saint Venant torsion theory to a 3D domain by considering the longitudinal direction. The newly proposed interface warping can consider geometries and material properties of both adjacent cross-sections of a given interface. Of course, for cross-sections without longitudinal discontinuity, the proposed torsion theory provides free warping functions obtained by solving the classical Saint Venant torsion theory. Using the finite element method, the proposed torsion theory is discretized to numerically calculate the interface warping functions. Unlike the method proposed by Yoon and Lee (2014a), Lagrangian multipliers are not needed.

In this study, we employ the interface warping functions in the formulation of continuum-mechanics based beams. To represent the entire warping displacement in the beam element, free and interface warping functions are adopted in continuous cross-sections and discontinuous interfaces, respectively. The developed beam finite element can predict complicated behaviors of beams with geometric and material discontinuities in the longitudinal direction. The compatibility of warping displacement is completely satisfied at the interface cross-section where longitudinal discontinuity occurs. Furthermore, partially constrained boundary conditions can be modeled utilizing the interface warping functions. Unlike the previous work by Yoon and Lee (2014a), no additional DOFs are required to model warping for discontinuous interface, and geometric nonlinear formulation can be directly obtained. That is, only 7 DOFs per node are utilized in the beam element. Nevertheless, more accurate solutions are obtained.

In the following sections, we first extend the classical

Saint Venant torsion theory to obtain the new interface warping functions. Then, the finite element discretization scheme is introduced to numerically calculate the warping functions. The continuum-mechanics based beam element equipped with new interface warping functions is explained. Finally, the performance of the beam finite element is demonstrated through several numerical examples considering both linear and nonlinear analysis.

2. Interface warping functions

Fig. 1 shows an example of a beam with cross-sectional discontinuity and its warping functions. The beam has three different cross-sections: ①, ②, and an interface cross-section between them. The classical Saint Venant torsion theory provides free warping functions for continuous cross-sections, as shown in Fig. 1(b). However, it is difficult to calculate the warping functions at an interface cross-section where discontinuity occurs. The main reason is that the cross-sections adjacent to the interface can have different geometric and material properties, but the classical Saint Venant theory can only handle continuous cross-sections.

Here, we present a new method to calculate the interface warping functions. Considering the longitudinal direction, the classical Saint Venant torsion theory given in the 2D domain is extended to a 3D domain. The governing equations in strong and weak forms are derived and finite element discretization is used to numerically calculate the interface warping functions.

2.1 Governing equations

Let us consider a straight infinite beam subjected to torsion. The beam can have both material and geometric discontinuities in the middle; thus, its twisting center can vary. Fig. 2(a) shows the finite beam domain Ω near the discontinuity, and the global Cartesian coordinate system is defined where the x-direction and the yz-plane are normal and parallel to the cross-sections, respectively. Assume that

(a) Global coordinate system and varying twisting center   (b) Cross-section with twisting center
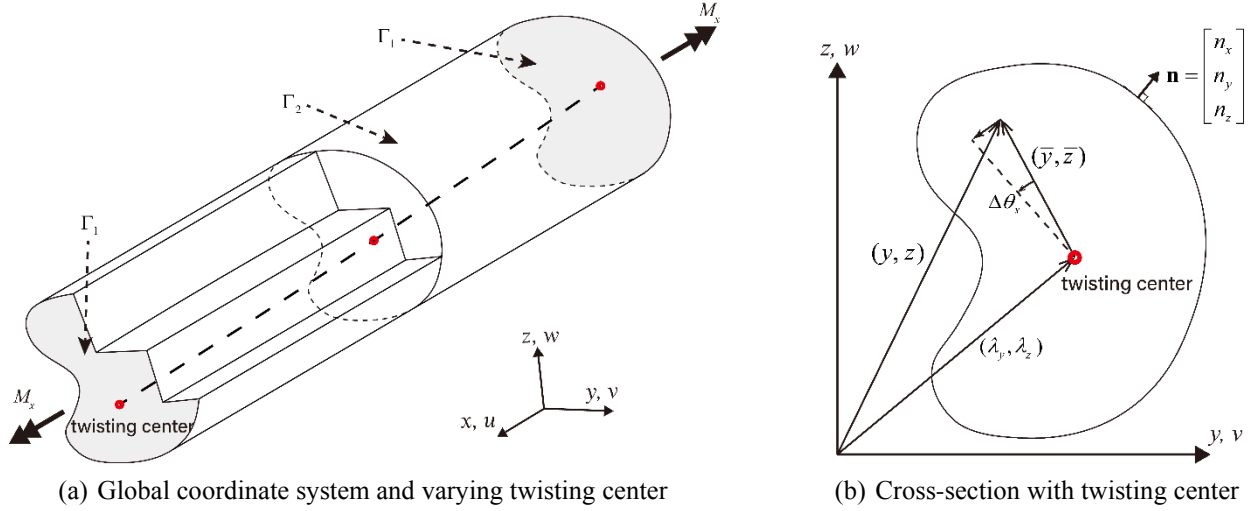
Fig. 2 Illustration of a straight beam with discontinuity

cross-sectional warping is allowed, but cross-sectional in-plane distortion is neglected.

Let us consider a cross-section rigidly rotating around its twisting center (λ_y, λ_z), as shown in Fig. 2(b). The corresponding displacements u, v, and w are defined with the following relations

$$u = f\alpha, \tag{1a}$$

$$\frac{\partial v}{\partial x} = -\bar{z}\alpha, \tag{1b}$$

$$\frac{\partial w}{\partial x} = \bar{y}\alpha, \tag{1c}$$

where $\bar{y} = y - \lambda_y(x)$, $\bar{z} = z - \lambda_z(x)$, and $f(x, y, z)$ is the warping function, and $\alpha(x) = \partial\theta_x/\partial x$ is the twist rate which is the angle of twist per unit length along the x-direction (Batoz and Dhatt 1990, Iesan 2008).

Without body force, the equilibrium equation of beam domain Ω is written as

$$\frac{\partial \sigma_{xx}}{\partial x} + \frac{\partial \sigma_{yx}}{\partial y} + \frac{\partial \sigma_{zx}}{\partial z} = 0 \text{ in } \Omega, \tag{2}$$

where σ_{xx}, σ_{yx}, and σ_{zx} are non-zero stress components.

The boundary Γ of beam domain Ω can be divided into two boundaries (Γ_1 and Γ_2 in Fig. 2(a)). The cross-sectional boundaries Γ_1 (gray colored), positioned at both ends of the domain, are normal to the x-axis and exposed to a torsional moment M_x. Although discontinuity exists in the middle, for a 'sufficiently (or infinitely)' long domain Ω, Saint Venant's principle guarantees that the x-directional component of traction (T_x) becomes zero on the cross-sectional boundaries Γ_1. On the lateral boundaries Γ_2, the x-directional component of traction (T_x) is zero since no external force is applied. As a result, on all boundaries

$$T_x = \sigma_{xx} n_x + \sigma_{yx} n_y + \sigma_{zx} n_z = 0 \text{ on } \Gamma, \tag{3}$$

in which n_x, n_y, and n_z are components of the unit vector ($\boldsymbol{n} = n_x \mathbf{e}_x + n_y \mathbf{e}_y + n_z \mathbf{e}_z$) normal to the boundary Γ.

Considering the linear elastic isotropic material law and the strain-displacement relation, the following equations are

obtained

$$\sigma_{xx} = E\varepsilon_{xx} = E\frac{\partial u}{\partial x}, \tag{4a}$$

$$\sigma_{yx} = 2G\varepsilon_{yx} = G\left(\frac{\partial u}{\partial y} + \frac{\partial v}{\partial x}\right), \tag{4b}$$

$$\sigma_{zx} = 2G\varepsilon_{zx} = G\left(\frac{\partial u}{\partial z} + \frac{\partial w}{\partial x}\right), \tag{4c}$$

where G is the shear modulus, E is Young's modulus, and ε_{xx}, ε_{yx}, and ε_{zx} are strain components.

By incorporating Eq. (1a)-(1c) and Eqs. (4a)-(4c) into Eq. (2) and Eq. (3), we obtain

$$E\frac{\partial^2 u}{\partial x^2} + G\frac{\partial^2 u}{\partial y^2} + G\frac{\partial^2 u}{\partial z^2} = 0 \text{ in } \Omega, \tag{5a}$$

$$\begin{aligned} G\left(\frac{E}{G}\frac{\partial u}{\partial x} n_x + \frac{\partial u}{\partial y} n_y + \frac{\partial u}{\partial z} n_z\right) \\ = -G\left(\frac{\partial v}{\partial x} n_y + \frac{\partial w}{\partial x} n_z\right) \text{ on } \Gamma. \end{aligned} \tag{5b}$$

Note that the twisting center (λ_y, λ_z) can vary along the x-direction inside the domain Ω, as shown in Fig. 2(a).

Unlike the classical Saint Venant torsion theory, the longitudinal displacement u becomes a function of x, and $\partial u/\partial x$ is no longer zero near the discontinuity. However, for a 'sufficiently (or infinitely)' long domain Ω, Eq. (3) and Eq. (4a) show $\partial u/\partial x = 0$ on the cross-sectional boundaries where n_x is not zero. Therefore, using a coordinate transformation, Eqs. (5a)-(5b) can be rearranged into Laplace's equation with the Neumann boundary condition as follows

$$G\left(\frac{\partial^2 u}{\partial \hat{x}^2} + \frac{\partial^2 u}{\partial \hat{y}^2} + \frac{\partial^2 u}{\partial \hat{z}^2}\right) = 0 \text{ in } \widehat{\Omega}, \tag{6a}$$

$$\begin{aligned} G\left(\frac{\partial u}{\partial \hat{x}}\hat{n}_x + \frac{\partial u}{\partial \hat{y}}\hat{n}_y + \frac{\partial u}{\partial \hat{z}}\hat{n}_z\right) \\ = -G\sqrt{\frac{G}{E}}\left(\frac{\partial v}{\partial \hat{x}}\hat{n}_y + \frac{\partial w}{\partial \hat{x}}\hat{n}_z\right) \text{ on } \widehat{\Gamma}, \end{aligned} \tag{6b}$$

in which $\hat{x} = \sqrt{\frac{G}{E}}x$, $\hat{y} = y$, and $\hat{z} = z$ are new coordinates, and $\widehat{\Omega}$ and $\widehat{\Gamma}$ denote the corresponding

transformed domain and its boundary, respectively.

The weak form of Eqs. (6a)-(6b) is derived with the virtual warping displacement field δu

$$\int_{\widehat{\Omega}} G\widehat{\mathbf{\nabla}} u \cdot \widehat{\mathbf{\nabla}} \delta u \, d\widehat{\Omega} = -\int_{\widehat{\Gamma}} G\sqrt{\frac{G}{E}} \left(\frac{\partial v}{\partial \hat{x}} \hat{n}_y + \frac{\partial w}{\partial \hat{x}} \hat{n}_z \right) \delta u \, d\widehat{\Gamma}, \quad (7)$$

where $\widehat{\mathbf{\nabla}} = \frac{\partial}{\partial \hat{x}} \mathbf{e}_x + \frac{\partial}{\partial \hat{y}} \mathbf{e}_y + \frac{\partial}{\partial \hat{z}} \mathbf{e}_z$ is the del operator of the transformed coordinate.

Substituting Eq. (1) into Eq. (7), the variational form of the 3D Saint Venant equation is obtained in the original coordinate system

$$\int_{\Omega} G \left(\frac{E}{G} \frac{\partial (f\alpha)}{\partial x} \frac{\partial \delta u}{\partial x} + \frac{\partial (f\alpha)}{\partial y} \frac{\partial \delta u}{\partial y} + \frac{\partial (f\alpha)}{\partial z} \frac{\partial \delta u}{\partial z} \right) d\Omega = \int_{\Gamma} G \left(\alpha \lambda_y n_z - \alpha \lambda_z n_y \right) \delta u \, d\Gamma + \int_{\Gamma} G\alpha \left(z n_y - y n_z \right) \delta u \, d\Gamma. \quad (8)$$

The warping function f of Eq. (8) also contains stretching and bending modes. To extract only the warping mode, the following orthogonality conditions are applied

$$\int_A E(1\mathbf{e}_x) \cdot (f\mathbf{e}_x) dA = 0, \quad (9a)$$

$$\int_A E(y\mathbf{e}_x) \cdot (f\mathbf{e}_x) dA = 0, \quad (9b)$$

$$\int_A E(z\mathbf{e}_x) \cdot (f\mathbf{e}_x) dA = 0, \quad (9c)$$

in which A is the area of the cross-section, perpendicular to the beam.

Resultant forces can be calculated on the cross-section

$$F_y = \int_A \sigma_{yx} dA = 0, \quad (10a)$$

$$F_z = \int_A \sigma_{zx} dA = 0, \quad (10b)$$

$$M_x = \int_A (\bar{y}\sigma_{zx} - \bar{z}\sigma_{yx}) dA = \int_A (y\sigma_{zx} - z\sigma_{yx}) dA - \lambda_y \int_A \sigma_{zx} dA + \lambda_z \int_A \sigma_{yx} dA, \quad (10c)$$

in which F_y and F_z are shear forces in the y- and z-directions, and M_x is the torsional moment about twisting center acting on cross-sectional area A.

Substituting Eqs. (10a) and (10b) into Eq. (10c), the following equation is obtained

$$M_x = \int_A (y\sigma_{zx} - z\sigma_{yx}) dA, \quad (11)$$

and using Eq. (1) and Eqs. (4b)-(4c) in Eq. (11) gives

$$M_x = \int_A G \left(y \frac{\partial (f\alpha)}{\partial z} - z \frac{\partial (f\alpha)}{\partial y} \right) dA -\alpha \lambda_y \int_A Gy dA - \alpha \lambda_z \int_A Gz dA + \alpha \int_A G(y^2 + z^2) dA. \quad (12)$$

2.2 Finite element discretization

To numerically calculate the interface warping function, here we present the finite element discretization of Eq. (8), Eqs. (9a)-(9c), and Eq. (12).

Let us introduce three unknown variables: $\tilde{\lambda}_y = \alpha \lambda_y$, $\tilde{\lambda}_z = \alpha \lambda_z$, and the warping displacement field $u = f\alpha$. Then, Eq. (8), Eqs. (9a)-(9c), and Eq. (12) become

$$\int_{\Omega} G \left(\frac{E}{G} \frac{\partial u}{\partial x} \frac{\partial \delta u}{\partial x} + \frac{\partial u}{\partial y} \frac{\partial \delta u}{\partial y} + \frac{\partial u}{\partial z} \frac{\partial \delta u}{\partial z} \right) d\Omega$$
$$= \int_{\Gamma} G \left(\tilde{\lambda}_y n_z - \tilde{\lambda}_z n_y \right) \delta u \, d\Gamma \quad (13a)$$
$$+ \int_{\Gamma} G\alpha \left(z n_y - y n_z \right) \delta u \, d\Gamma,$$

$$\int_A E(1\mathbf{e}_x) \cdot (u\mathbf{e}_x) dA = 0, \quad (13b)$$

$$\int_A E(y\mathbf{e}_x) \cdot (u\mathbf{e}_x) dA = 0, \quad (13c)$$

$$\int_A E(z\mathbf{e}_x) \cdot (u\mathbf{e}_x) dA = 0, \quad (13d)$$

$$M_x = \int_A G \left(y \frac{\partial u}{\partial z} - z \frac{\partial u}{\partial y} \right) dA$$
$$-\tilde{\lambda}_y \int_A Gy dA - \tilde{\lambda}_z \int_A Gz dA + \alpha \int_A G(y^2 + z^2) dA. \quad (13e)$$

The 3D beam domain Ω in Fig. 2(a) is discretized using a 3D finite element model, as shown in Fig. 3(a)

$$\Omega = \bigcup_{e=1}^{d} \Omega^{(e)}, \quad (14)$$

in which $\Omega^{(e)}$ denotes the 3D finite element domains and d is the number of finite elements used. Different material properties can be assigned in each finite element domain to model composite beams.

Each domain $\Omega^{(e)}$ consists of a p-node solid element. The displacement function $u^{(e)}$ in the finite element domain $\Omega^{(e)}$ is interpolated as

$$u^{(e)}(x, y, z) = \mathbf{H}^{(e)} \mathbf{U}^{(e)} \quad (15)$$

with

$$\mathbf{U}^{(e)} = \left[u_1^{(e)}, \cdots, u_i^{(e)}, \cdots, u_p^{(e)} \right]^T, \quad (16a)$$

$$\mathbf{H}^{(e)} = \left[H_1(x, y, z), \cdots, H_i(x, y, z), \cdots, H_p(x, y, z) \right], \quad (16b)$$

where $u_i^{(e)}$ is the nodal warping displacement value at node i, $\mathbf{U}^{(e)}$ is the vector containing the nodal warping displacement values, $H_i(x, y, z)$ is the 3D shape functions corresponding to node i, and $\mathbf{H}^{(e)}$ is the matrix containing the shape functions.

Similarly, the virtual warping displacement field $\delta u^{(e)}$ is interpolated as

$$\delta u^{(e)}(x, y, z) = \mathbf{H}^{(e)} \delta \mathbf{U}^{(e)} \quad (17)$$

with

$$\delta \mathbf{U}^{(e)} = \left[\delta u_1^{(e)}, \cdots, \delta u_i^{(e)}, \cdots, \delta u_p^{(e)} \right]^T, \quad (18)$$

where $\delta \mathbf{U}^{(e)}$ is the vector containing the virtual nodal warping displacement values, $\delta u_i^{(e)}$.

Fig. 3(b) illustrates the internal and external boundaries of the finite element domain $\Omega^{(e)}$: $\Gamma^{(e)} = \Gamma_{\text{int}}^{(e)} \cup \Gamma_{\text{ext}}^{(e)}$ with internal boundary $\Gamma_{\text{int}}^{(e)}$ (colored in blue) and external boundary $\Gamma_{\text{ext}}^{(e)}$ (colored in red). The boundary of the entire domain Ω is denoted by
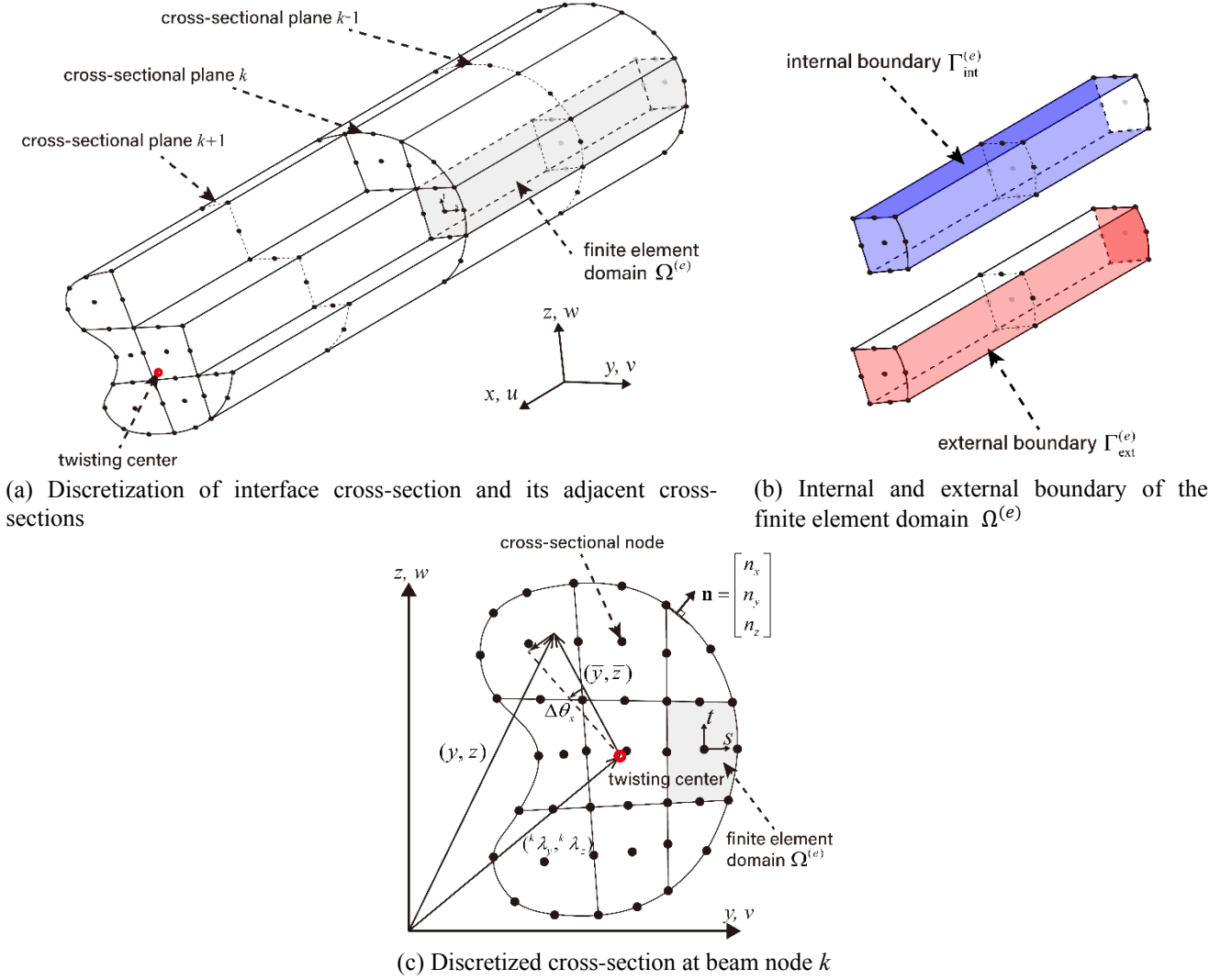
$$\Gamma = \bigcup_{e=1}^{d} \Gamma_{\text{ext}}^{(e)}. \quad (19)$$

Each cross-sectional plane of sub-beam e rotates around its twisting center, as shown in Fig. 3(c). The variables $(\tilde{\lambda}_y, \tilde{\lambda}_z)$ are interpolated as

$$\tilde{\lambda}_y(x) = \mathbf{h}^{(e)} \widetilde{\mathbf{\Lambda}}_y^{(e)}, \quad \tilde{\lambda}_z(x) = \mathbf{h}^{(e)} \widetilde{\mathbf{\Lambda}}_z^{(e)}, \quad (20)$$

with

$$\widetilde{\mathbf{\Lambda}}_y^{(e)} = \left[{}^1\tilde{\lambda}_y^{(e)}, \cdots, {}^l\tilde{\lambda}_y^{(e)}, \cdots, {}^q\tilde{\lambda}_y^{(e)} \right]^T, \quad (21a)$$

(a) Discretization of interface cross-section and its adjacent cross-sections

(b) Internal and external boundary of the finite element domain $\Omega^{(e)}$

(c) Discretized cross-section at beam node k

Fig. 3 Discretization of the beam domain Ω for interface warping calculation

$$\widetilde{\boldsymbol{\Lambda}}_z^{(e)} = \begin{bmatrix} {}^1\tilde{\lambda}_z^{(e)}, & \cdots, & {}^l\tilde{\lambda}_z^{(e)}, & \cdots, & {}^q\tilde{\lambda}_z^{(e)} \end{bmatrix}^T, \tag{21b}$$

$$\mathbf{h}^{(e)} = \begin{bmatrix} h_1(x), & \cdots, & h_l(x), & \cdots, & h_q(x) \end{bmatrix}, \tag{21c}$$

where q is the number of the cross-sectional planes of sub-beam e, $({}^l\tilde{\lambda}_y^{(e)}, {}^l\tilde{\lambda}_z^{(e)})$ denotes the variables $(\tilde{\lambda}_y, \tilde{\lambda}_z)$ of the lth cross-sectional plane of sub-beam e, $\widetilde{\boldsymbol{\Lambda}}_y^{(e)}$ and $\widetilde{\boldsymbol{\Lambda}}_z^{(e)}$ are the vectors containing ${}^l\tilde{\lambda}_y^{(e)}$ and ${}^l\tilde{\lambda}_z^{(e)}$, respectively, and $\mathbf{h}^{(e)}$ is the matrix containing 1D shape functions, $h_l(x)$, corresponding to cross-sectional plane l.

Similarly, the twist rate α is interpolated using the same 1D shape function

$$\alpha(x) = \mathbf{h}^{(e)}\mathbf{A}^{(e)}, \tag{22}$$

with

$$\mathbf{A}^{(e)} = \begin{bmatrix} {}^1\alpha^{(e)}, & \cdots, & {}^l\alpha^{(e)}, & \cdots, & {}^q\alpha^{(e)} \end{bmatrix}^T, \tag{23}$$

where ${}^l\alpha^{(e)}$ denotes the twist rate of the lth cross-sectional plane of sub-beam e.

Using Eqs. (14)-(23) in Eq. (13a), the following finite element discretization is obtained

$$\delta\mathbf{U}^T \mathbf{A}_{e=1}^d \Big[\int_{\Omega^{(e)}} G^{(e)} \Big(\frac{E^{(e)}}{G^{(e)}} \frac{\partial \mathbf{H}^{(e)T}}{\partial x} \frac{\partial \mathbf{H}^{(e)}}{\partial x}$$

$$+ \frac{\partial \mathbf{H}^{(e)T}}{\partial y} \frac{\partial \mathbf{H}^{(e)}}{\partial y} + \frac{\partial \mathbf{H}^{(e)T}}{\partial z} \frac{\partial \mathbf{H}^{(e)}}{\partial z}\Big) d\Omega\Big] \mathbf{U}$$

$$- \delta\mathbf{U}^T \mathbf{A}_{e=1}^d \Big[\int_{\Gamma_{ext}^{(e)}} G^{(e)} \mathbf{H}^{(e)T} \mathbf{h}^{(e)} n_z \, d\Gamma\Big] \widetilde{\boldsymbol{\Lambda}}_y$$

$$+ \delta\mathbf{U}^T \mathbf{A}_{e=1}^d \Big[\int_{\Gamma_{ext}^{(e)}} G^{(e)} \mathbf{H}^{(e)T} \mathbf{h}^{(e)} n_y \, d\Gamma\Big] \widetilde{\boldsymbol{\Lambda}}_z$$

$$+ \delta\mathbf{U}^T \mathbf{A}_{e=1}^d \Big[\int_{\Gamma_{ext}^{(e)}} G^{(e)} \big(-zn_y + yn_z\big) \mathbf{H}^{(e)T} \mathbf{h}^{(e)} d\Gamma\Big] \mathbf{A}$$

$$= \mathbf{0} \tag{24}$$

where $\mathbf{U}$, $\delta\mathbf{U}$, $\widetilde{\boldsymbol{\Lambda}}_y$, $\widetilde{\boldsymbol{\Lambda}}_z$, and $\mathbf{A}$ are the vectors containing $\mathbf{U}^{(e)}$, $\delta\mathbf{U}^{(e)}$, $\widetilde{\boldsymbol{\Lambda}}_y^{(e)}$, $\widetilde{\boldsymbol{\Lambda}}_z^{(e)}$, and $\mathbf{A}^{(e)}$ of all finite element domains, respectively, and A is the assembly operator (Hughes 2000).

For an infinitely long domain, the change of warping displacements along the x-direction is negligible compared to the change along the y- and z-directions: $\frac{\partial \mathbf{H}}{\partial x} \ll \frac{\partial \mathbf{H}}{\partial y}$ and $\frac{\partial \mathbf{H}}{\partial x} \ll \frac{\partial \mathbf{H}}{\partial z}$

$$\delta \mathbf{U}^T \mathbf{A}_{e=1}^d \left[\int_{\Omega^{(e)}} G^{(e)} \left(\frac{\partial \mathbf{H}^{(e)T}}{\partial y} \frac{\partial \mathbf{H}^{(e)}}{\partial y} + \frac{\partial \mathbf{H}^{(e)T}}{\partial z} \frac{\partial \mathbf{H}^{(e)}}{\partial z} \right) d\Omega \right] \mathbf{U}$$

$$- \mathbf{U}^T \mathbf{A}_{e=1}^d \left[\int_{\Gamma_{\text{ext}}^{(e)}} G^{(e)} \mathbf{H}^{(e)T} \mathbf{h}^{(e)} n_z \, d\Gamma \right] \widetilde{\mathbf{\Lambda}}_y$$

$$+ \delta \mathbf{U}^T \mathbf{A}_{e=1}^d \left[\int_{\Gamma_{\text{ext}}^{(e)}} G^{(e)} \mathbf{H}^{(e)T} \mathbf{h}^{(e)} n_y \, d\Gamma \right] \widetilde{\mathbf{\Lambda}}_z \qquad (25)$$

$$+ \delta \mathbf{U}^T \mathbf{A}_{e=1}^d \left[\int_{\Gamma_{\text{ext}}^{(e)}} G^{(e)} \left(-z n_y + y n_z \right) \mathbf{H}^{(e)T} \mathbf{h}^{(e)} d\Gamma \right] \mathbf{A}$$

$$= \mathbf{0}.$$

Note that the length of the domain Ω no longer affects the solution of Eq. (25), because all the integrals in the equation are linearly proportional to the length of the domain. Therefore, the domain length can be arbitrarily chosen when calculating the interface warping functions.

By eliminating $\delta \mathbf{U}$ in Eq. (25), the following equation in matrix form is obtained

$$\mathbf{K}_w \mathbf{U} - \mathbf{N}_z \widetilde{\mathbf{\Lambda}}_y + \mathbf{N}_y \widetilde{\mathbf{\Lambda}}_z + \mathbf{B}_c \mathbf{A} = \mathbf{0} \qquad (26)$$

with

$$\mathbf{K}_w = \mathbf{A}_{e=1}^d \left[\int_{\Omega^{(e)}} G^{(e)} \left(\frac{\partial \mathbf{H}^{(e)T}}{\partial y} \frac{\partial \mathbf{H}^{(e)}}{\partial y} + \frac{\partial \mathbf{H}^{(e)T}}{\partial z} \frac{\partial \mathbf{H}^{(e)}}{\partial z} \right) d\Omega \right], (27a)$$

$$\mathbf{N}_z = \mathbf{A}_{e=1}^d \left[\int_{\Gamma_{\text{ext}}^{(e)}} G^{(e)} n_z \mathbf{H}^{(e)T} \mathbf{h}^{(e)} \, d\Gamma \right], \qquad (27b)$$

$$\mathbf{N}_y = \mathbf{A}_{e=1}^d \left[\int_{\Gamma_{\text{ext}}^{(e)}} G^{(e)} n_y \mathbf{H}^{(e)T} \mathbf{h}^{(e)} \, d\Gamma \right], \qquad (27c)$$

$$\mathbf{B}_c = \mathbf{A}_{e=1}^d \left[\int_{\Gamma_{\text{ext}}^{(e)}} G^{(e)} \left(-z n_y + y n_z \right) \mathbf{H}^{(e)T} \mathbf{h}^{(e)} d\Gamma \right]. \quad (27d)$$

The orthogonality conditions of Eqs. (13b)-(13d) are also discretized and expressed in the matrix and vector forms

$$\mathbf{Q}_x \mathbf{U} = \mathbf{0}, \ \mathbf{Q}_y \mathbf{U} = \mathbf{0}, \ \mathbf{Q}_z \mathbf{U} = \mathbf{0}, \qquad (28)$$

with

$$\mathbf{Q}_x = \mathbf{A}_{e=1}^d \left[\int_{\Omega^{(e)}} E^{(e)} \mathbf{H}_1^{(e)T} d\Omega, \cdots, \int_{\Omega^{(e)}} E^{(e)} \mathbf{H}_n^{(e)T} d\Omega \right]^T, \quad (29a)$$

$$\mathbf{Q}_y = \mathbf{A}_{e=1}^d \left[\int_{\Omega^{(e)}} y E^{(e)} \mathbf{H}_1^{(e)T} d\Omega, \cdots, \int_{\Omega^{(e)}} y E^{(e)} \mathbf{H}_n^{(e)T} d\Omega \right]^T, \quad (29b)$$

$$\mathbf{Q}_z = \mathbf{A}_{e=1}^d \left[\int_{\Omega^{(e)}} z E^{(e)} \mathbf{H}_1^{(e)T} d\Omega, \cdots, \int_{\Omega^{(e)}} z E^{(e)} \mathbf{H}_n^{(e)T} d\Omega \right]^T, \quad (29c)$$

where $\mathbf{H}_k^{(e)}$ is the 3D interpolation matrix $\mathbf{H}^{(e)}$ at cross-sectional plane k.

Eq. (13e) is discretized and expressed in matrix form as follow

$$\mathbf{R}_w \mathbf{U} - \mathbf{S}_y \widetilde{\mathbf{\Lambda}}_y - \mathbf{S}_z \widetilde{\mathbf{\Lambda}}_z + \mathbf{J}_x \mathbf{A} = M_x \mathbf{1}, \qquad (30)$$

with

$$\mathbf{R}_w = \mathbf{A}_{e=1}^d \left[\mathbf{C}_1^{(e)}, \mathbf{C}_2^{(e)}, \cdots, \mathbf{C}_k^{(e)}, \cdots, \mathbf{C}_n^{(e)} \right]^T, \qquad (31a)$$

$$\mathbf{S}_y = \mathbf{A}_{e=1}^d \left[\int_{\Omega^{(e)}} G^{(e)} y \mathbf{h}_k^{(e)T} \mathbf{h}_k^{(e)} \, d\Omega \right], \qquad (31b)$$

$$\mathbf{S}_z = \mathbf{A}_{e=1}^d \left[\int_{\Omega^{(e)}} G^{(e)} z \mathbf{h}_k^{(e)T} \mathbf{h}_k^{(e)} d\Omega \right], \qquad (31c)$$

$$\mathbf{J}_x = \mathbf{A}_{e=1}^d \left[\int_{\Omega^{(e)}} G^{(e)} (y^2 + z^2) \mathbf{h}_k^{(e)T} \mathbf{h}_k^{(e)} d\Omega \right], \qquad (31d)$$

$$\mathbf{1} = [1, 1, \cdots, 1]^T, \qquad (31e)$$

where $\mathbf{h}_k^{(e)}$ is the 1D interpolation matrix $\mathbf{h}^{(e)}$ at cross-sectional plane k, M_x is an torsional moment acting on the beam, and $\mathbf{C}_k^{(e)}$ is defined as

$$\mathbf{C}_k^{(e)} = \left[\int_{\Omega^{(e)}} G^{(e)} \left(y \frac{\partial \mathbf{H}_k^{(e)T}}{\partial z} - z \frac{\partial \mathbf{H}_k^{(e)T}}{\partial y} \right) d\Omega \right]. \qquad (31f)$$

Eqs. (26)-(31) can be merged into the following matrix equation

$$\begin{bmatrix} \mathbf{K}_w & -\mathbf{N}_z & \mathbf{N}_y & \mathbf{B}_c \\ \mathbf{Q}_x & 0 & 0 & 0 \\ \mathbf{Q}_y & 0 & 0 & 0 \\ \mathbf{Q}_z & 0 & 0 & 0 \\ \mathbf{R}_w & -\mathbf{S}_y & -\mathbf{S}_z & \mathbf{J}_x \end{bmatrix} \begin{bmatrix} \mathbf{U} \\ \widetilde{\mathbf{\Lambda}}_y \\ \widetilde{\mathbf{\Lambda}}_z \\ \mathbf{A} \end{bmatrix} = M_x \begin{bmatrix} \mathbf{0} \\ \mathbf{0} \\ \mathbf{0} \\ \mathbf{0} \\ \mathbf{1} \end{bmatrix}. \qquad (32)$$

Solving Eq. (32), the interface warping function, the corresponding twisting center, and the twist rate can be simultaneously calculated along with the fully coupled effects of adjacent elements. Since the magnitude of M_x is proportional to the twist rate and does not affect the warping function and twisting center, an arbitrary number can be applied to M_x. Note that, when Eq. (32) is applied to continuous cross-section beams with uniform material, the free warping function with constant twist rate and twisting center is obtained.

We tested the proposed finite element discretization to calculate the interface warping function considering beams with geometric and material discontinuities. Almost the same interface warping functions were calculated irrespective of beam length and number of elements used along the longitudinal direction. Therefore, the use of only two elements along the longitudinal direction is recommended. For example, considering the beam in Fig. 1, one element is used for cross-section ① and another element is used for cross-section ②.
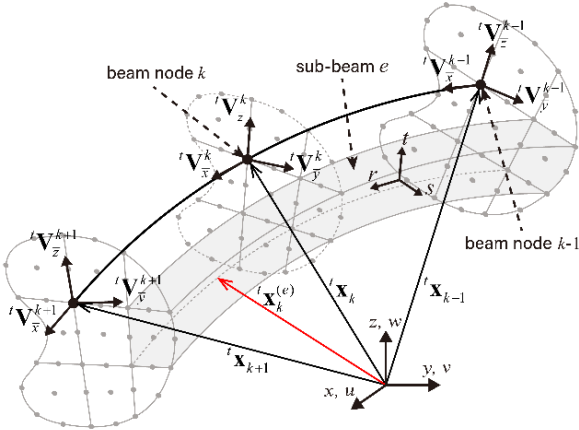
3. Continuum-mechanics based beam element

In this section, we present the implementation of the interface warping function in the beam finite element formulation. To consider the warping displacement, a continuum-mechanics based beam element is employed, which is directly degenerated from an assemblage of 3D solid finite elements (Yoon and Lee 2014a, Bathe 1996, Kim *et al.* 2020, Kim *et al.* 2021, Yoon *et al.* 2012, Yoon and Lee 2014b, Yoon *et al.* 2015, Yoon *et al.* 2017a, b). As shown in Fig. 4(a), an arbitrary-shaped continuum-mechanics based beam element consists of multiple sub-beams. Note that a superscript t indicates incremental load levels, and its corresponding configurations in static nonlinear analysis rather than actual time in dynamic analysis (Yoon *et al.* 2012, Yoon and Lee 2014b, Yoon *et al.* 2015, Yoon *et al.* 2017a, b).

Fig. 4(b) shows the *n*-node continuum-mechanics based
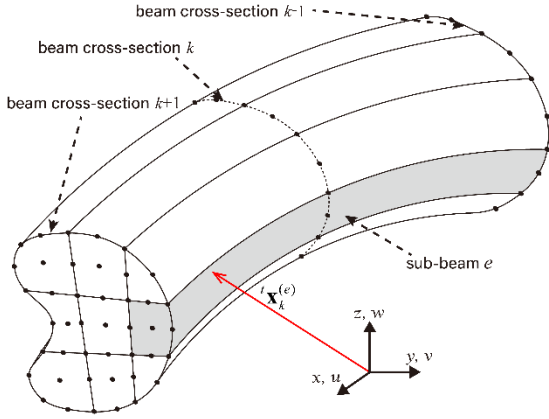
(a) 3-node arbitrary-shaped curved beam with sub-beams

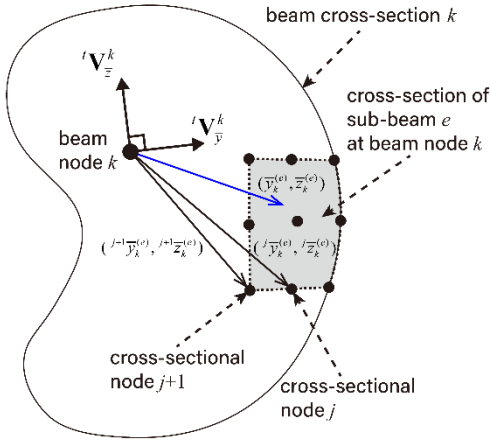(b) Continuum-mechanics based beam element with beam nodes and director vectors

(c) Cross-sectional Cartesian coordinate system at beam node k, at time t

Fig. 4 Concept of the continuum-mechanics based beam element

beam element with its nodes and director vectors. Inside the sub-beam e (gray color in Fig. 4), a material position in the configuration at time t can be written as

$$
{}^t\boldsymbol{x}^{(e)} = \sum_{k=1}^{n} h_k(r)\big({}^t\boldsymbol{x}_k + \bar{y}_k^{(e)}\, {}^t\mathbf{V}_{\bar{y}}^k + \bar{z}_k^{(e)}\, {}^t\mathbf{V}_{\bar{z}}^k + \bar{f}_k^{(e)}\, {}^t\mathbf{V}_{\bar{x}}^k\, {}^t\alpha_k \big),
\tag{33}
$$

where $h_k(r)$ is the 1D shape function corresponding to

beam node k, ${}^t\boldsymbol{x}_k$ is the position vector of beam node k, ${}^t\mathbf{V}_{\bar{y}}^k$ and ${}^t\mathbf{V}_{\bar{z}}^k$ are orthonormal director vectors to define the cross-sectional Cartesian coordinate system at beam node k, $\bar{y}_k^{(e)}(s,t)$ and $\bar{z}_k^{(e)}(s,t)$ denote the coordinates in the cross-sectional Cartesian coordinate system on cross-sectional plane k, ${}^t\mathbf{V}_{\bar{x}}^k(= {}^t\mathbf{V}_{\bar{y}}^k \times {}^t\mathbf{V}_{\bar{z}}^k)$ is the warping director vector orthonormal to the cross-section, $\bar{f}_k^{(e)}$ is the warping function value on cross-sectional plane k, and ${}^t\alpha_k$ is the corresponding warping DOF at beam node k.

Fig. 4(c) shows the cross-sectional geometry in the cross-sectional Cartesian coordinate system at beam node k. For an m-node cross-sectional element corresponding to sub-beam e (colored in gray), the material position and the warping function are interpolated as

$$
\bar{y}_k^{(e)} = \sum_{j=1}^{m} h_j(s,t)\, {}^j\bar{y}_k^{(e)},
\tag{34a}
$$

$$
\bar{z}_k^{(e)} = \sum_{j=1}^{m} h_j(s,t)\, {}^j\bar{z}_k^{(e)},
\tag{34b}
$$

$$
\bar{f}_k^{(e)} = \sum_{j=1}^{m} h_j(s,t)\, {}^j f_k^{(e)},
\tag{34c}
$$

where $h_j(s,t)$ is the 2D shape function corresponding to cross-sectional node j, ${}^j\bar{y}_k^{(e)}$ and ${}^j\bar{z}_k^{(e)}$ denote the position of cross-sectional node j, and ${}^j f_k^{(e)}$ is the warping function value at cross-sectional node j. Note that ${}^j f_k^{(e)}$ is pre-calculated through Eq. (32).

From the geometry interpolation in Eq. (33), the incremental displacement field of sub-beam e from time t to $t + \Delta t$ is obtained as

$$
\begin{aligned}
{}_0\mathbf{u}^{(e)} = \sum_{k=1}^{n} h_k\big[{}_0\mathbf{u}_k + {}_0\alpha_k \bar{f}_k^{(e)}\, {}_0\mathbf{R}_k \mathbf{V}_{\bar{x}}^k \\
+ \big({}_0\mathbf{R}_k - \mathbf{I} \big)\big(\bar{y}_k^{(e)}\, {}^t\mathbf{V}_{\bar{y}}^k + \bar{z}_k^{(e)}\, {}^t\mathbf{V}_{\bar{z}}^k + {}^t\alpha_k \bar{f}_k^{(e)}\, {}^t\mathbf{V}_{\bar{x}}^k \big)\big],
\end{aligned}
\tag{35}
$$

where ${}_0\mathbf{u}_k$, ${}_0\boldsymbol{\theta}^k$ and ${}_0\alpha_k$ are the incremental nodal DOFs at beam node k consisting of three translations, three rotations and warping, respectively, and ${}_0\mathbf{R}_k({}_0\boldsymbol{\theta}^k)$ is the finite rotation tensor of beam node k from time t to $t + \Delta t$ (Yoon *et al.* 2012, Yoon and Lee 2014b, Yoon *et al.* 2015, Yoon *et al.* 2017a, b) defined as

$$
{}^{t+\Delta t}\mathbf{V}_{\bar{x}}^k = {}_0\mathbf{R}_k\, {}^t\mathbf{V}_{\bar{x}}^k,
\tag{36a}
$$

$$
{}^{t+\Delta t}\mathbf{V}_{\bar{y}}^k = {}_0\mathbf{R}_k\, {}^t\mathbf{V}_{\bar{y}}^k,
\tag{36b}
$$

$$
{}^{t+\Delta t}\mathbf{V}_{\bar{z}}^k = {}_0\mathbf{R}_k\, {}^t\mathbf{V}_{\bar{z}}^k.
\tag{36c}
$$

The position and displacement fields are then used to derive the linearized incremental equilibrium equation for nonlinear incremental analysis based on the total Lagrangian formulation. The equation is discretized using nodal DOFs, and its solutions are calculated iteratively and incrementally. The calculated DOFs are used to update the position and director vectors of each node in every incremental step. Detailed nonlinear formulations are well described in Bathe (1996), Yoon *et al.* (2012), Yoon and Lee (2014b), Yoon *et al.* (2015), Yoon *et al.* (2017a, b).
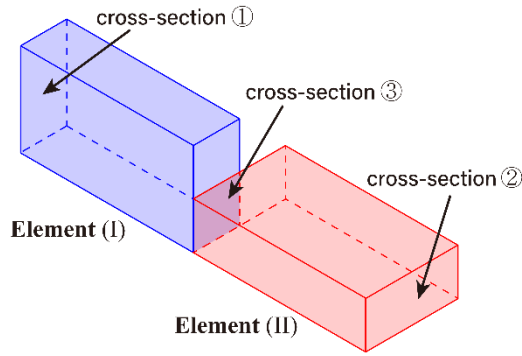
(a) Beam with longitudinal discontinuity and its cross-sections
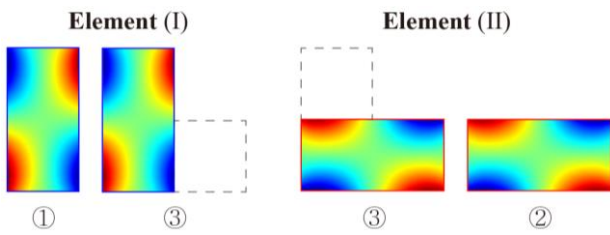
(b) Free warping beam model constructed using free warping functions
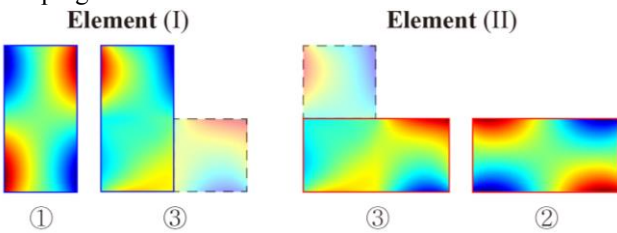
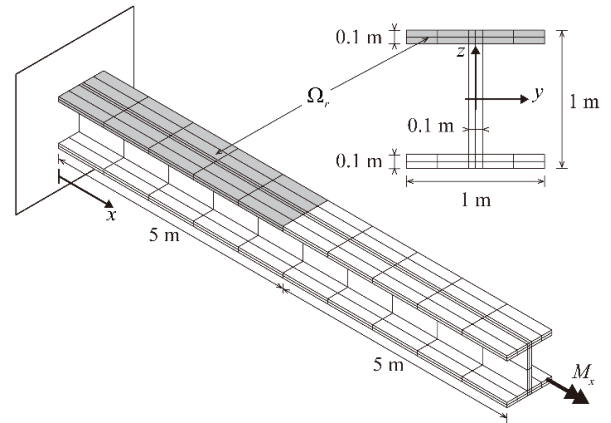(c) Proposed warping beam model constructed using the interface warping function

Fig. 5 Comparison of the free warping beam model and the proposed warping beam model

(a) Reference solid model
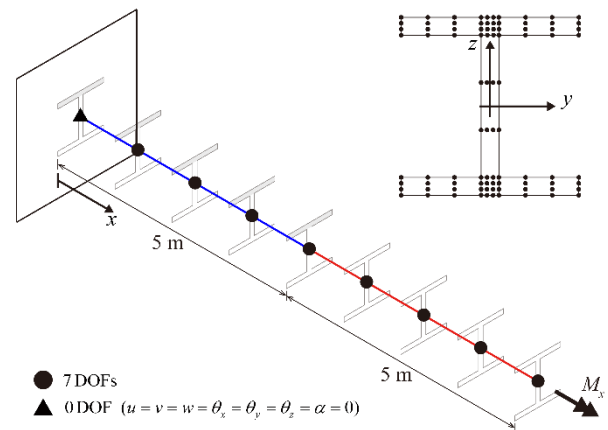

(b) Beam model and its cross-sectional mesh

Fig. 6 Partially reinforced wide flange beam

4. Numerical examples

In this section, we present four numerical examples to verify the usefulness of the proposed interface warping function: a partially reinforced wide flange beam, a partially constrained warping problem, a step varying rectangular cross-section beam, and a circular beam with a step varying rectangular cross-section.

In the following examples, the beams are modeled using 2-node continuum-mechanics based beam elements, and their cross-sections are discretized using 4-node or 16-node quadrilateral cross-sectional elements. The well-known reduced integration scheme is applied along the longitudinal direction of the beam element to avoid shear locking (Hughes 2000, Bathe 1996), and 2×2 or 4×4 Gauss integration points are used on 4-node or 16-node cross-sectional elements, respectively. The interface warping functions are calculated using Eq. (32) in the straight beam domain Ω in Fig. 3(a), where its cross-sectional mesh used is the same as that of continuum-mechanics based beam elements.

Fig. 5 compares two different methods of modeling beams with longitudinal discontinuity. Fig. 5(a) illustrates

two beam elements, (I) and (II), with three different cross-sections: ①, ②, and ③. Fig. 5(b) shows the free warping beam model, in which free warping functions of each cross-section are applied to each node. In this model, the compatibility of warping displacements is not satisfied at the interface cross-section ③. This incompatibility can be resolved with the proposed warping beam model by applying the interface warping function to cross-section ③, as shown in Fig. 5(c). As a result, the adjacent elements of the interface cross-section share the same warping shape and magnitude; therefore, the displacement compatibility is always satisfied.

The numerical results are compared with the reference solutions obtained using 20-node hexahedral solid elements in ANSYS (ANSYS 2017). To assess the performance of the proposed warping beam model, the calculated values using the free warping beam model, BEAM188 in ANSYS, and results from Yoon and Lee (2014a) are compared. While BEAM188, the free warping beam model, and the proposed warping beam model employ 7 DOFs per node, 7 to 9 DOFs per node are used in the beam model by Yoon and Lee (2014a).

4.1 Partially reinforced wide flange beam

Here, we consider a partially reinforced wide flange

(a) Free warping displacement and twisting center $(\lambda_y, \lambda_z) = (0, 0.2234)$ at $x = 2.5$ m

(b) Interface warping displacement and twisting center $(\lambda_y, \lambda_z) = (0, 0.1487)$ at $x = 5.0$ m

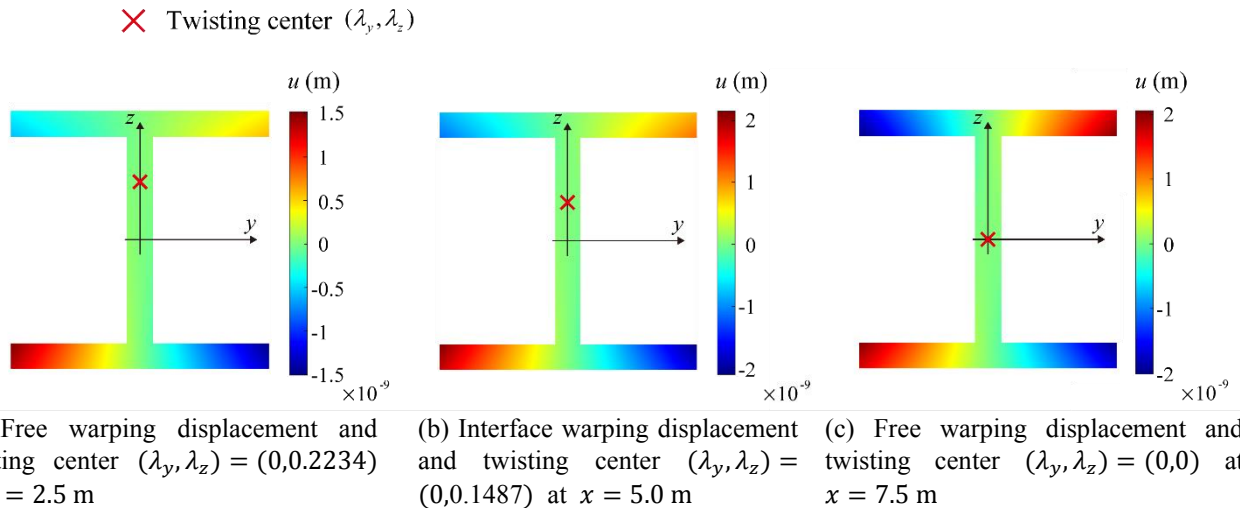(c) Free warping displacement and twisting center $(\lambda_y, \lambda_z) = (0, 0)$ at $x = 7.5$ m

Fig. 7 Distributions of the warping displacements u and twisting centers (λ_y, λ_z) for the partially reinforced wide flange beam. The location of twisting centers is indicated by a red cross

(a) Twist angle θ_x

(b) Displacement v of point A along the beam

(c) Displacement v of point B along the beam
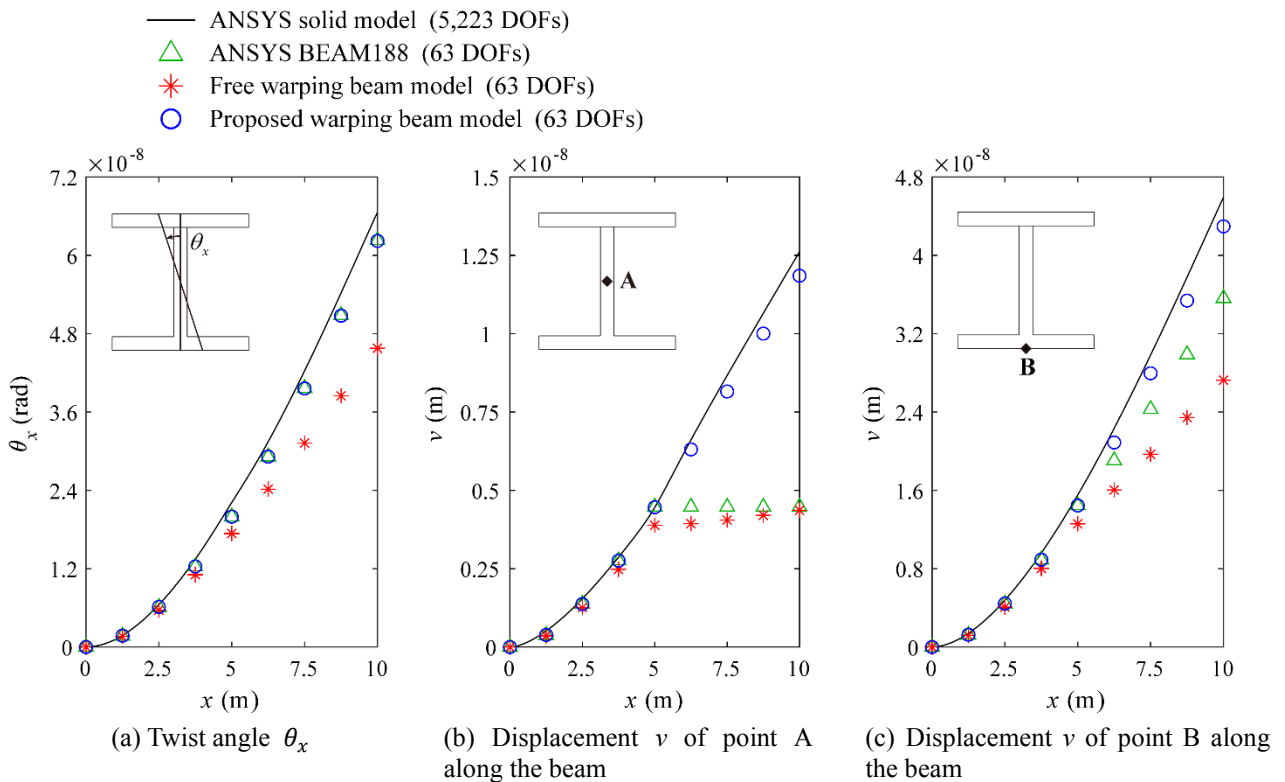
Fig. 8 Linear analysis results for the partially reinforced wide flange beam

beam of length 10 m with material discontinuity. As shown in Fig. 6(a), the height and width of the cross-section are 1m, and the thickness is 0.1 m. Half of the beam has a reinforced upper flange Ω_r (colored in gray) with Young's modulus $E_r = 6 \times 10^{11}$ Pa and Poisson's ratio $\nu = 0$, as illustrated in Fig. 6(a). In the remaining part, Young's modulus is $E_0 = 2 \times 10^{11}$ Pa and Poisson's ratio is $\nu = 0$. The beam is fully clamped at $x = 0$ m and the torsional moment M_x is applied at $x = 10$ m.

To obtain the reference solutions, the solid model is constructed using 280 hexahedral solid elements (5,223 DOFs), as illustrated in Fig. 6(a). All DOFs are fixed at the

clamped end surface ($x = 0$ m), and the torsional moment M_x is applied at the free end surface ($x = 10$ m). Three beam models are constructed using eight 2-node beam elements ($7 \times 9 = 63$ DOFs) for comparison: an ANSYS beam model using BEAM188, a free warping beam model, and the proposed warping beam model. The fully clamped boundary condition ($u = v = w = \theta_x = \theta_y = \theta_z = \alpha = 0$) is applied at $x = 0$ m, as shown in Fig. 6(b). The cross-section of the ANSYS BEAM188 is discretized with twenty-eight 9-node quadratic cross-sectional elements, and the proposed warping beam model is discretized with seven 16-node cubic cross-sectional elements.
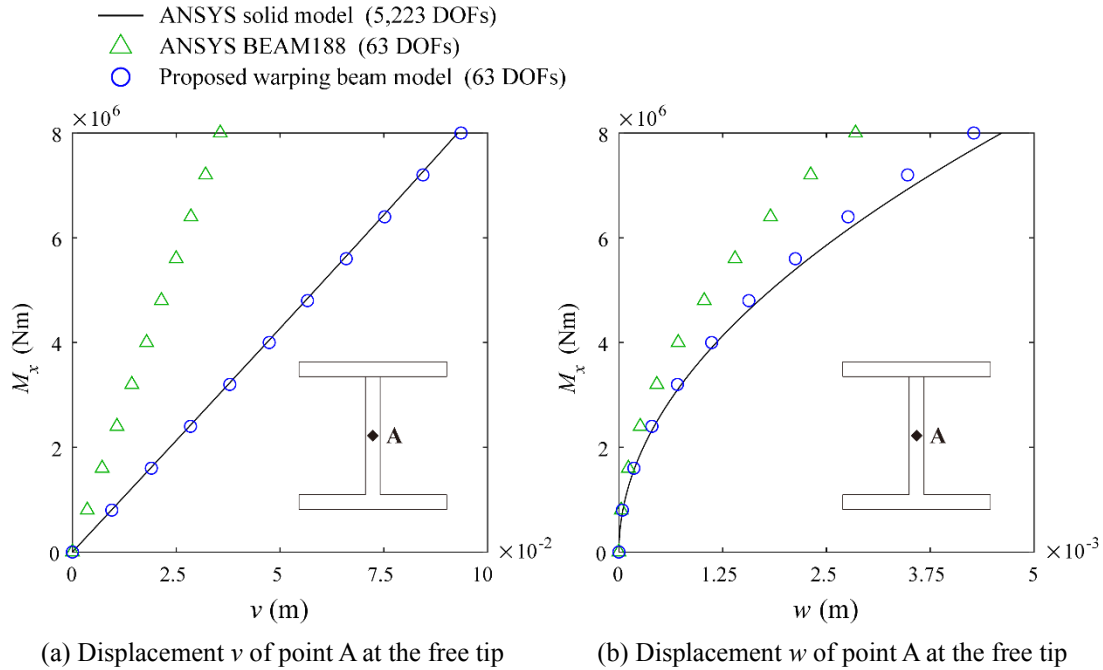
— ANSYS solid model (5,223 DOFs)
△ ANSYS BEAM188 (63 DOFs)
○ Proposed warping beam model (63 DOFs)

(a) Displacement v of point A at the free tip   (b) Displacement w of point A at the free tip

Fig. 9 Load-displacement curves for the partially reinforced wide flange beam

— ANSYS solid model (5,223 DOFs)
△ ANSYS BEAM188 (63 DOFs)
○ Proposed warping beam model (63 DOFs)

(a) Displacement v of point A at the free tip   (b) Displacement w of point A at the free tip
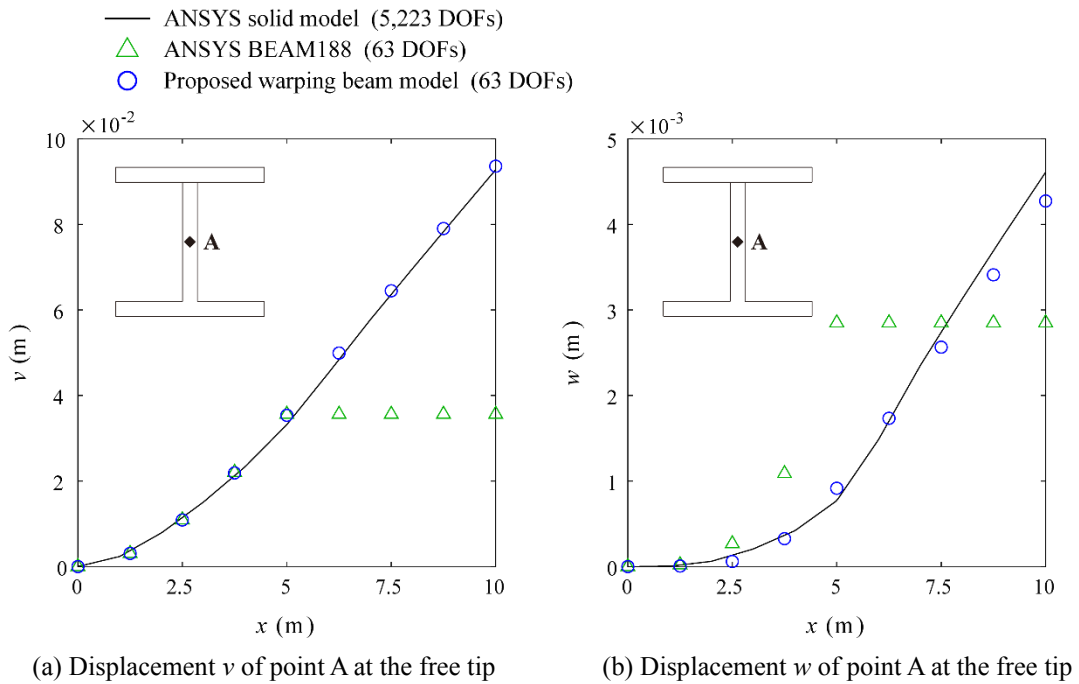
Fig. 10 Nonlinear analysis results for the partially reinforced wide flange beam

Fig. 7 illustrates the distribution of the calculated warping displacements and positions of the twisting centers at $x = 2.5$ m, $x = 5.0$ m, and $x = 7.5$ m when $M_x = 1$ Nm is applied. The shape of free warping displacements and the corresponding positions of twisting centers at $x = 2.5$ m and $x = 7.5$ m are identical to those from the classical Saint Venant torsion theory. However, the interface warping function at $x = 5.0$ m can only be obtained through Eq. (32). The variation of the twisting center along the x-direction is automatically considered through the displacement field in Eq. (33).

Fig. 8 compares three numerical results of the linear analysis along the beam length when $M_x = 1$ Nm is applied: the distribution of twist angle θ_x and y-directional displacements v of points A and B, respectively. The proposed warping beam model shows good agreement with the reference model, while the free warping beam model fails to predict the behavior of the beam after the interface ($x = 5$ m). ANSYS BEAM188 gives a twist angle that exhibits superb agreement with the reference solutions, but displacements corresponding to points A and B do not match with the reference solutions.
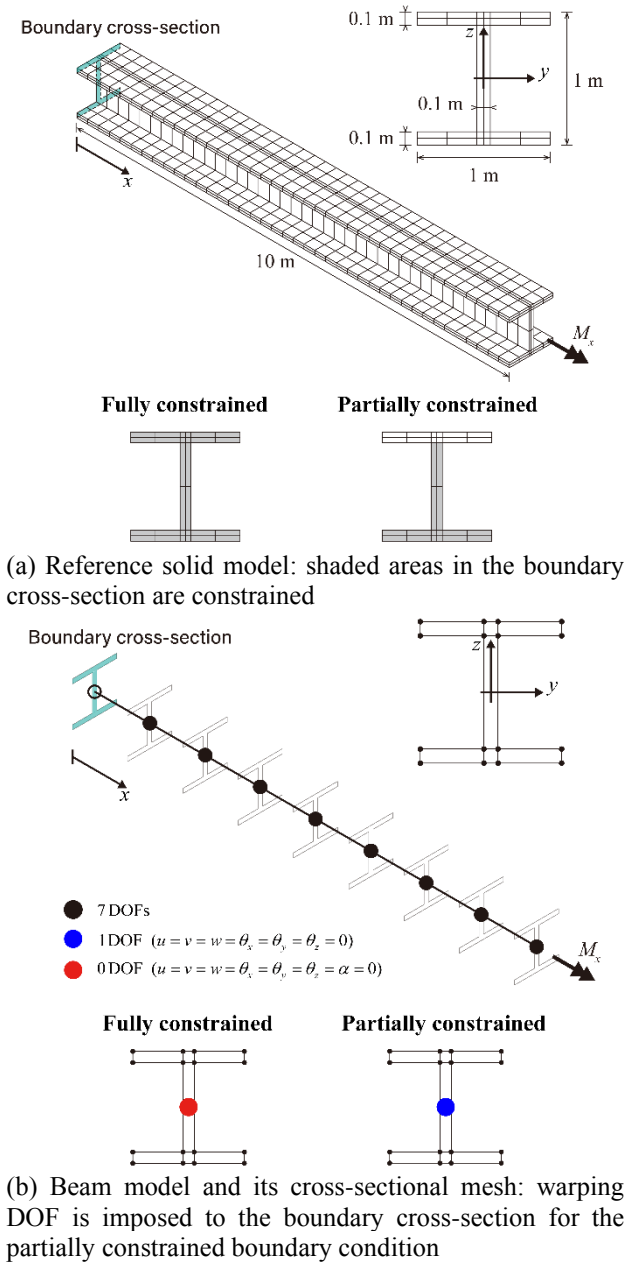
(a) Reference solid model: shaded areas in the boundary cross-section are constrained

(b) Beam model and its cross-sectional mesh: warping DOF is imposed to the boundary cross-section for the partially constrained boundary condition

(c) Model used to calculate the interface warping function by attaching a rigid beam

Fig. 11 Partially constrained warping problem

For geometric nonlinear analysis, the torsional moment M_x increases up to 8×10^6 Nm. Fig. 9 displays the load-displacement curves, where the displacements of point A at the free tip is considered. This shows the proposed warping beam model can accurately predict the deformation due to
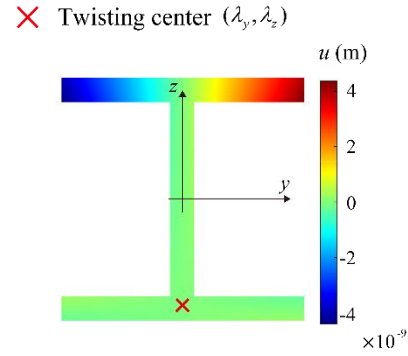
(a) Interface warping displacement and twisting center $(\lambda_y, \lambda_z) = (0, -0.4369)$ at $x = 0.0$ m
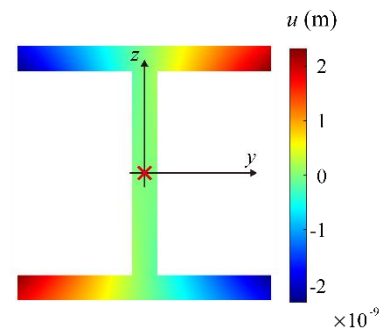
(b) Free warping displacement and twisting center $(\lambda_y, \lambda_z) = (0,0)$ at $x = 5.0$ m

Fig. 12 Distributions of the warping displacements u and twisting centers (λ_y, λ_z) for the constrained warping problem. The location of twisting centers is indicated by a red cross

the twisting-bending coupling unlike ANSYS BEAM188. Fig. 10 illustrates the displacement distributions when the torsional moment of $M_x = 8 \times 10^6$ Nm is applied at the free tip. This shows that the proposed warping beam model can accurately predict not only the y-directional displacement v of point A, but also the z-directional displacement w of point A.

4.2 Partially constrained warping problem

In this section, we consider the wide flange beam proposed in Yoon and Lee (2014a). The geometry of the beam is equal to that used in the previous example.

In this problem, two boundary conditions are considered: a partially constrained boundary condition and a fully constrained boundary condition. In the boundary cross-section at $x = 0$ m, all displacements, including warping, are constrained only at the shaded area in Fig. 11(a), and a torsional moment M_x is applied at the free end ($x = 10$ m). Young's modulus is $E = 2 \times 10^{11}$ Pa and Poisson's ratio is $v = 0$.

The reference solid model uses 1,120 hexahedral solid elements (19,803 DOFs), as illustrated in Fig. 11(a). All nodes corresponding to the shaded area ($x = 0$ m) are fixed. Fig. 11(b) shows a beam model consisting of eight 2-node beam elements; its cross-section consists of seven 4-node cross-sectional elements. All DOFs at $x = 0$ m are fully
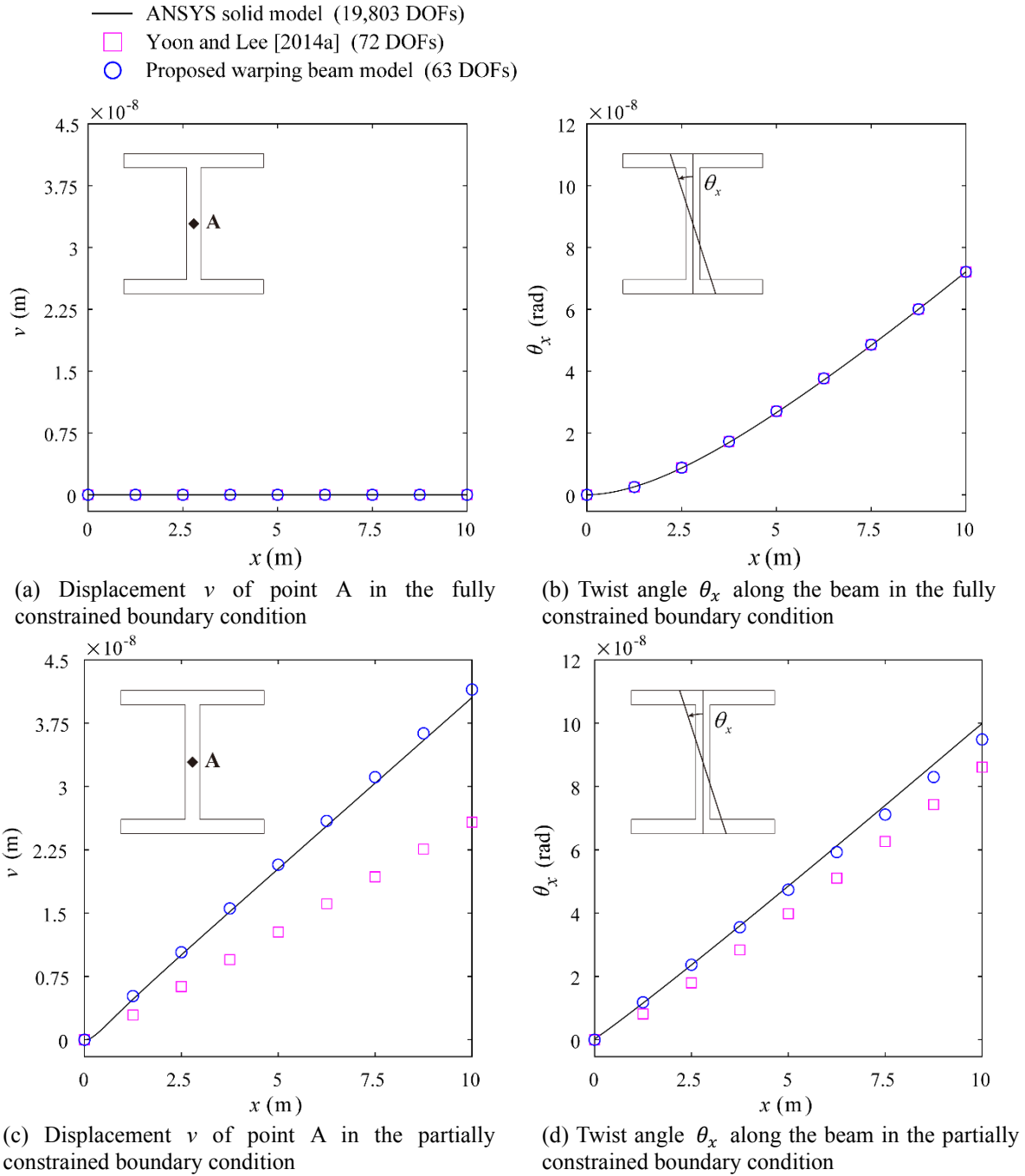
(a) Displacement v of point A in the fully constrained boundary condition

(b) Twist angle θ_x along the beam in the fully constrained boundary condition

(c) Displacement v of point A in the partially constrained boundary condition

(d) Twist angle θ_x along the beam in the partially constrained boundary condition

Fig. 13 Linear analysis results for the partially constrained warping problem in fully and partially constrained boundary conditions

clamped ($u = v = w = \theta_x = \theta_y = \theta_z = \alpha = 0$) for the fully constrained condition, while the partially constrained boundary condition has warping DOF ($u = v = w = \theta_x = \theta_y = \theta_z = 0$), as illustrated in Fig. 11(b). Note that Yoon and Lee (2014a) used 8 DOFs per node ($8 \times 9 = 72$ DOFs) to solve this beam problem, while the proposed warping beam model uses 7 DOFs per node ($7 \times 9 = 63$ DOFs).

The interface warping function is employed to model the partially constrained boundary condition. Fig. 11(c) shows the model used to calculate the interface warping function by attaching a rigid beam (colored in gray, Ω_r) to

the boundary cross-section. The rigid beam is modeled with a higher Young's modulus $E_r = 2 \times 10^{18}$ Pa and Poisson's ratio $v = 0$. Note that the model in Fig. 11(c) is only adopted to calculate the interface warping function using Eq. (32).

Fig. 12 demonstrates the distribution of the calculated warping displacements and positions of the twisting centers at $x = 0.0$ m and $x = 5.0$ m when $M_x = 1$ Nm is applied. The warping displacement at $x = 5.0$ m shows the free warping function, and its twisting center is located on $y = z = 0.0$ m due to symmetry. The shape of the warping displacement observed at $x = 0.0$ m is similar to
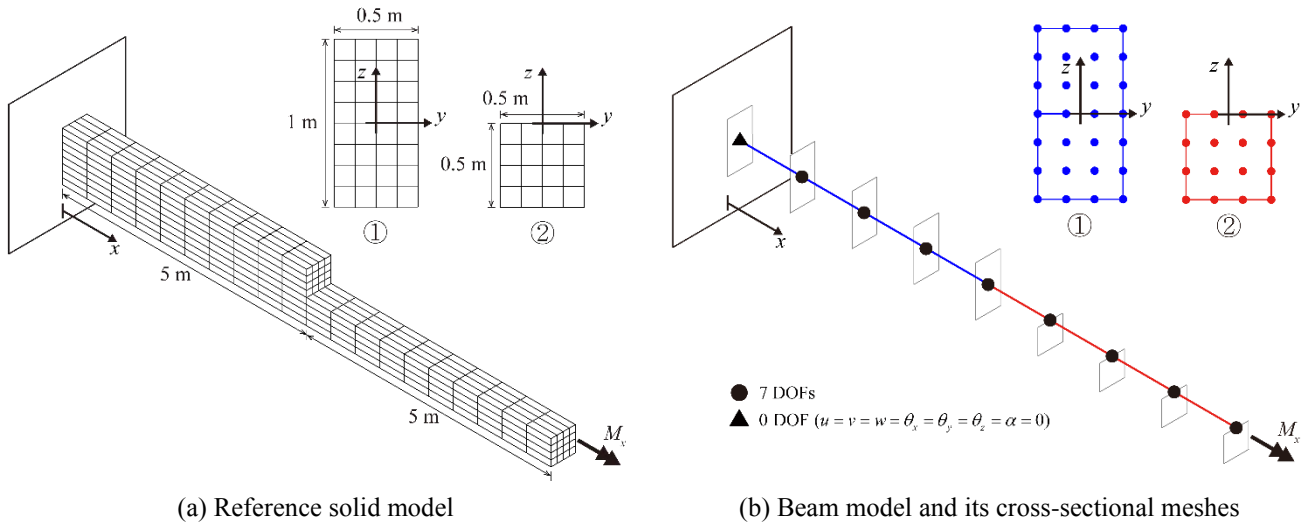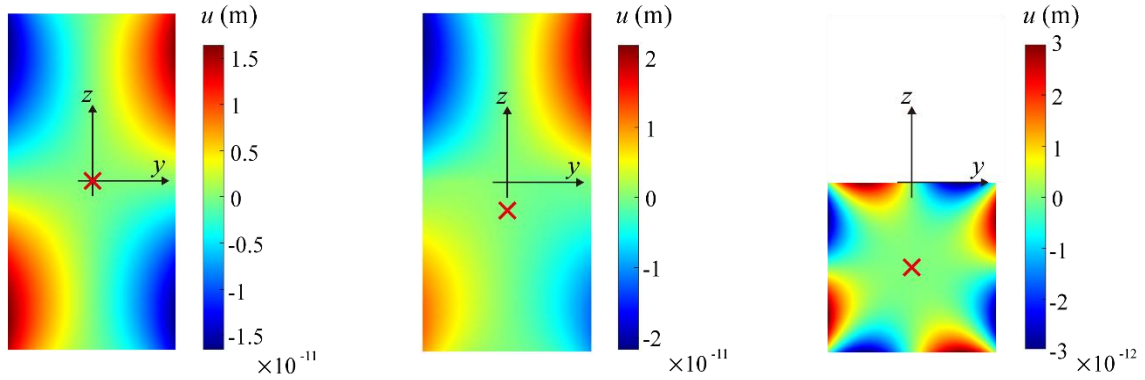
(a) Reference solid model   (b) Beam model and its cross-sectional meshes

Fig. 14 Step varying rectangular cross-section beam

(a) Free warping displacement and twisting center $(\lambda_y, \lambda_z) = (0,0)$ at $x = 0.0$ m

(b) Interface warping displacement and twisting center $(\lambda_y, \lambda_z) = (0, -0.0833)$ at $x = 5.0$ m

(c) Free warping displacement and twisting center $(\lambda_y, \lambda_z) = (0, -0.25)$ at $x = 7.5$ m

Fig. 15 Distributions of the warping displacements u and twisting centers (λ_y, λ_z) for the step varying rectangular cross-section beam. The location of twisting centers is indicated by a red cross

that of the free warping function except for the constrained region (shaded area in Fig. 11(a)), but the location of the twisting center is significantly different.

Fig. 13 shows the numerical results of the linear analysis when $M_x = 1$ Nm is applied at the free tip. In the fully constrained boundary condition, both results from Yoon and Lee (2014a) and the proposed warping beam model match considerably well with the reference solution. However, in the partially constrained boundary condition, even though the proposed warping beam model used fewer DOFs per node, it shows better results compared with those in Yoon and Lee (2014a). Note that the classical Saint Venant torsion theory cannot be applied to solve the partially constrained warping problems.

4.3 Step varying rectangular cross-section beam

Fig. 14(a) shows the step varying rectangular cross-section beam (Yoon and Lee 2014a) with two parts. Cross-sections of each beam part, ① and ②, have heights of 0.5 m and 1 m, respectively, and an identical width of 0.5 m. Young's modulus is $E = 2 \times 10^{11}$ Pa and Poisson's ratio is $\nu = 0$. A fully clamped boundary condition is imposed at $x = 0$ m while torsional moment M_x is applied at $x = 10$ m.

As illustrated in Fig. 14(a), the reference solid model is constructed using 480 hexahedral solid elements (8,055 DOFs). All DOFs are fixed at the clamped end surface ($x = 0$ m), and the torsional moment M_x is applied at the free end surface ($x = 10$ m). Fig. 14(b) shows that the beam models consist of eight 2-node beam elements, with cross-sections ① and ② (blue and red colored, respectively). 7 DOFs per node are used to construct the proposed warping beam and ANSYS BEAM188 models ($7 \times 9 = 63$ DOFs), but Yoon and Lee (2014a) used 7 and 8 DOFs per node to express the warping effect at the interface and continuous cross-sections, respectively (71 DOFs).
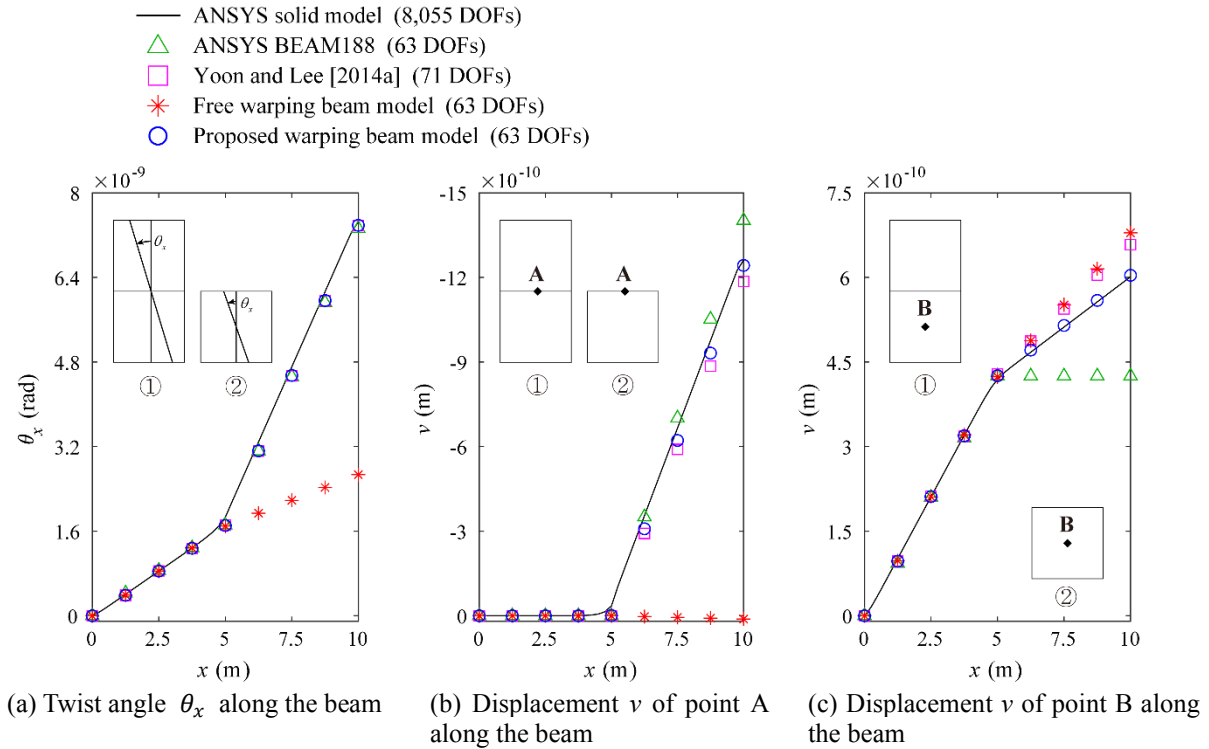
The proposed warping beam model used two and one

(a) Twist angle θ_x along the beam (b) Displacement v of point A along the beam (c) Displacement v of point B along the beam

Fig. 16 Linear analysis results for the step varying rectangular cross-section beam

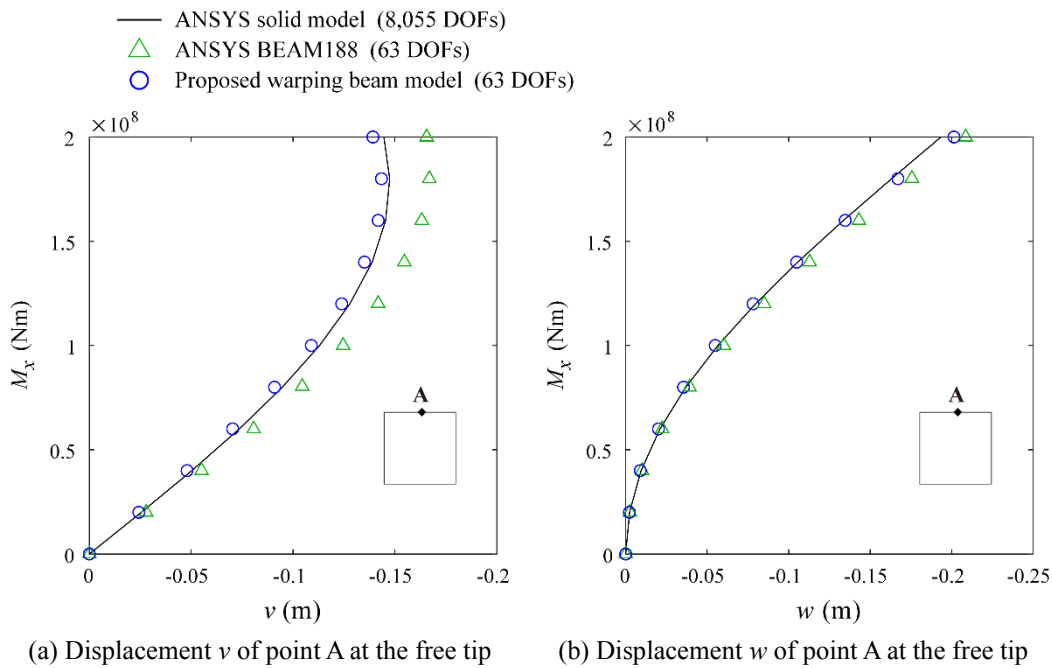(a) Displacement v of point A at the free tip (b) Displacement w of point A at the free tip

Fig. 17 Load-displacement curves for the step varying rectangular cross-section beam

16-node cross-sectional elements to discretize cross-sections ① and ②, respectively, as in Yoon and Lee (2014a). The cross-sections of the ANSYS BEAM188 model are discretized using finer meshes with eight and four 9-node quadratic cross-sectional elements, respectively. A fully constrained boundary condition ($u = v = w = \theta_x = \theta_y = \theta_z = \alpha = 0$) at $x = 0\,\mathrm{m}$ is applied and torsional moment M_x is applied at the free end.

Fig. 15 illustrates the calculated warping displacements and positions of twisting centers at $x = 2.5\,\mathrm{m}$, $x = 5.0\,\mathrm{m}$, and $x = 7.5\,\mathrm{m}$ of the proposed warping beam model, when $M_x = 1\,\mathrm{Nm}$ is applied. Fig. 16 presents the linear analysis results along the beam length when $M_x = 1\,\mathrm{Nm}$ is applied. It can be seen that the proposed warping beam model is the most reliable for analyzing the beam with discontinuity. We also confirm that the proposed warping beam model used fewer DOFs to express the warping effect but showed better accuracy compared to the results in Yoon
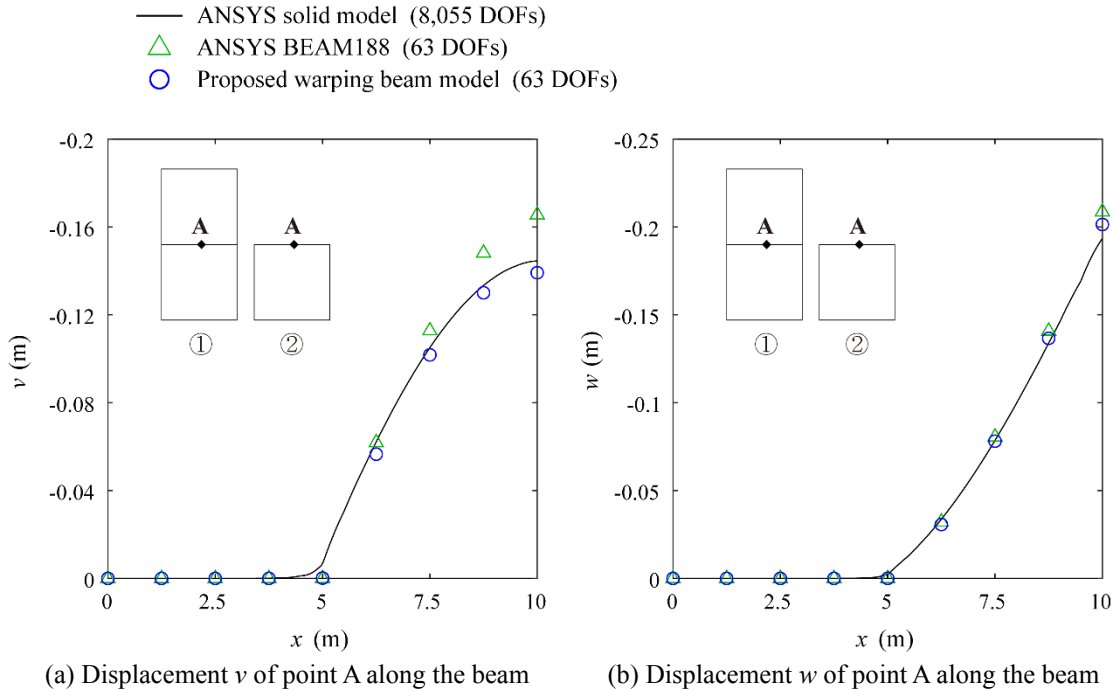
(a) Displacement *v* of point A along the beam   (b) Displacement *w* of point A along the beam

Fig. 18 Nonlinear analysis results for the step varying rectangular cross-section beam

(a) Reference solid model   (b) Beam model and its cross-sectional meshes
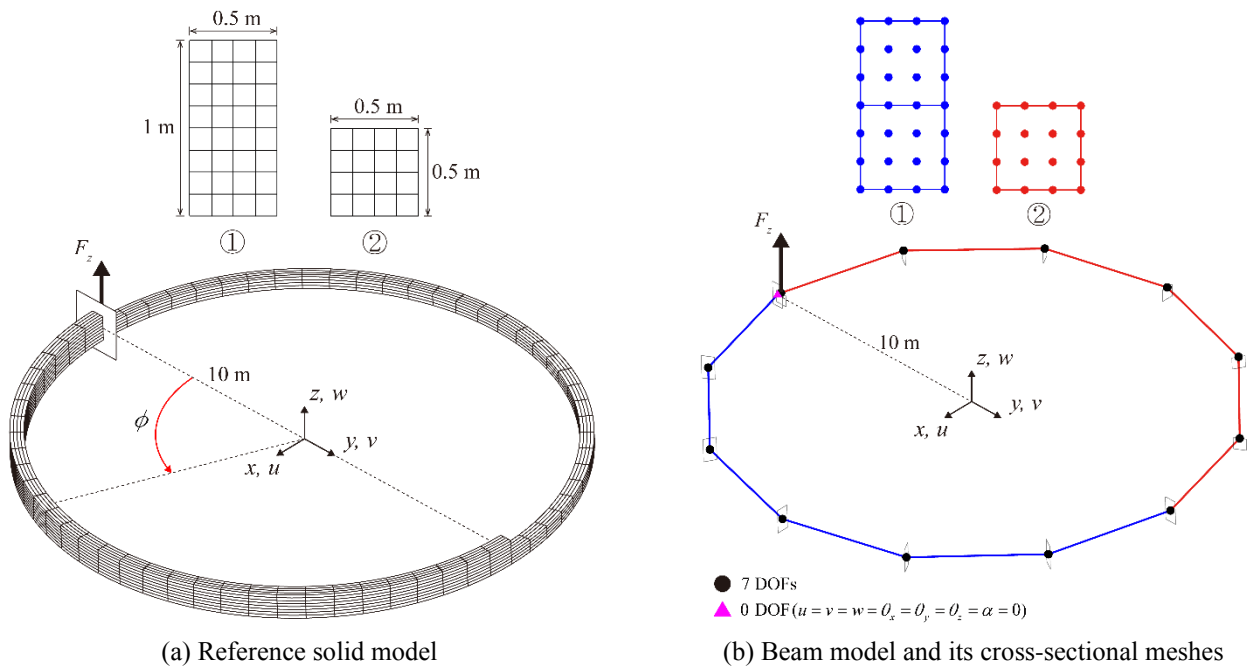
Fig. 19 Circular beam with a step varying rectangular cross-section

and Lee (2014a). The free warping beam model failed to predict the behavior of the beam after the interface cross-section.

For geometric nonlinear analysis, we statically increase the torsional moment M_x up to 2×10^8 Nm. Fig. 17 displays the load-displacement curves, where the displacements of point A at the free tip are considered when $M_x = 2 \times 10^8$ Nm is applied. The results indicate that the proposed warping beam model predicts the geometric nonlinear behavior better than the ANSYS BEAM188. Fig. 18 shows the displacements of point A along the beam

length when $M_x = 2 \times 10^8$ Nm is applied. As seen, the proposed warping beam model successfully reflects the twisting-bending coupling effect compared with the ANSYS BEAM188 model.

4.4 Circular beam with step varying rectangular cross-section

Finally, we consider the circular beam with a step varying rectangular cross-section, as shown in Fig. 19, to assess the twisting-bending behavior of the curved beam
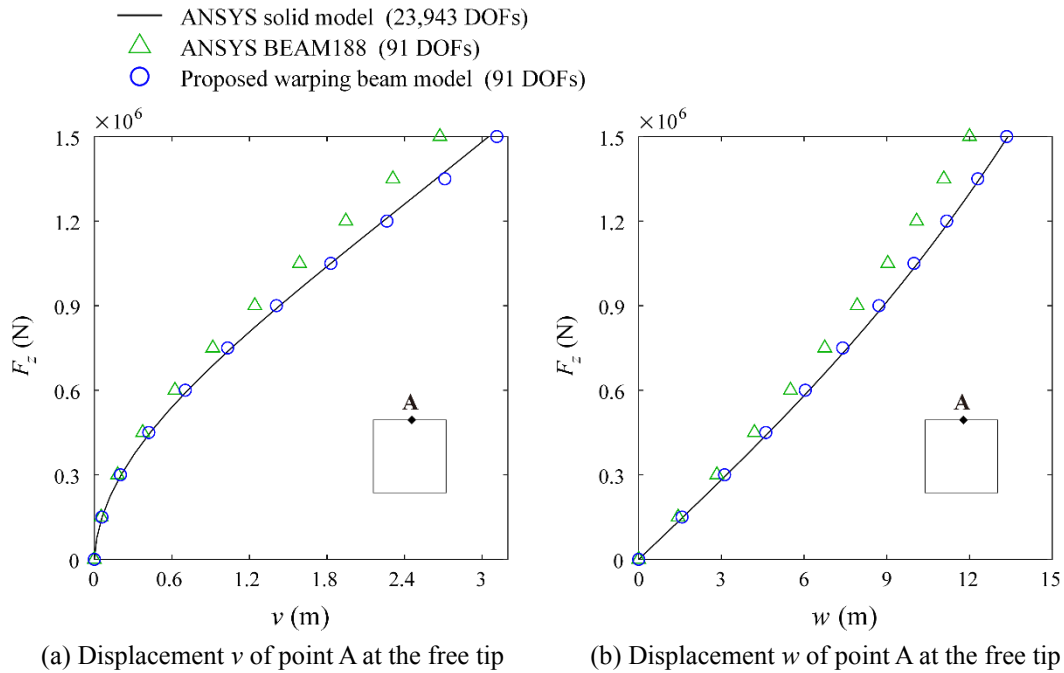
(a) Displacement *v* of point A at the free tip   (b) Displacement *w* of point A at the free tip

Fig. 20 Load-displacement curves for the circular beam with a step varying rectangular cross-section

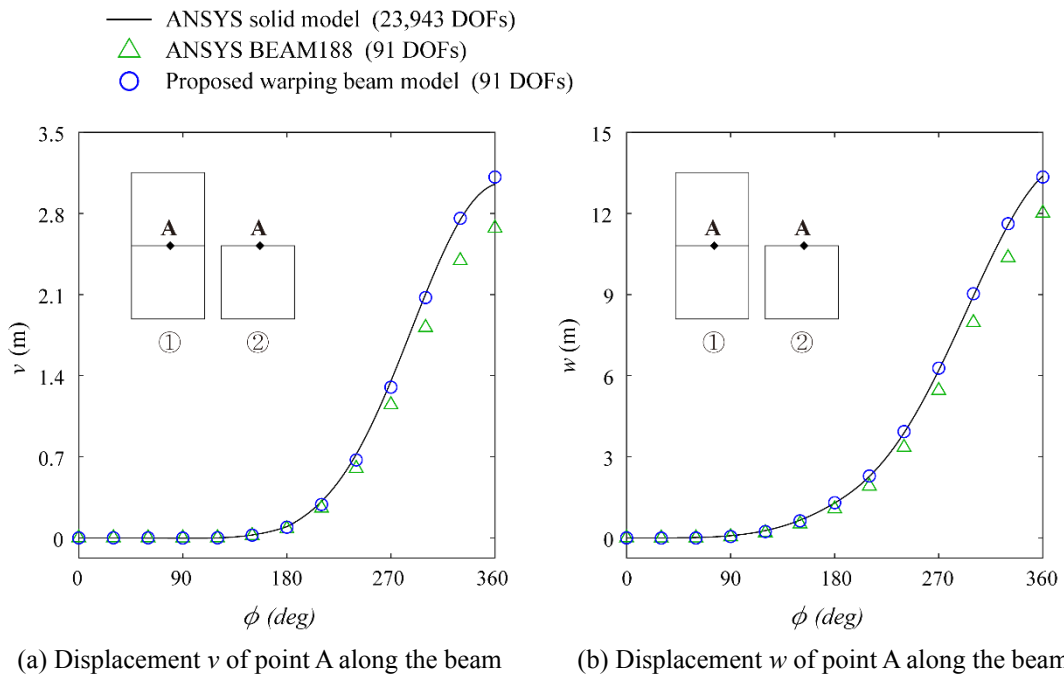(a) Displacement *v* of point A along the beam   (b) Displacement *w* of point A along the beam

Fig. 21 Nonlinear analysis results for the circular beam with a step varying rectangular cross-section

with longitudinal discontinuity. The beam has a radius of 10 m and its cross-section discontinuously varies from the rectangular cross-section ① to the square cross-section ② at $\phi = 180°$. The beam is fully clamped at $\phi = 0°$, and a force $F_z = 1.5 \times 10^6$ N is applied at $\phi = 359°$. Young's modulus is $E = 2 \times 10^{11}$ Pa and Poisson's ratio is $v = 0.3$. Geometric nonlinear analysis is performed, since the beam is expected to undergo large displacement and large rotation.

The reference solid model is obtained using 1,472 hexahedral solid elements (23,943 DOFs), as shown in Fig.

19(a). All DOFs are constrained at $\phi = 0°$, and the force $F_z = 1.5 \times 10^6$ N is applied at the free end surface ($\phi = 359°$). Fig. 19(b) shows that the beam model consists of twelve 2-node beam elements ($7 \times 13 = 91$ DOFs), which are used to construct both proposed warping beam and ANSYS BEAM188 models. The cross-sections ① and ② are discretized using eight and four 9-node quadratic cross-sectional elements for the ANSYS BEAM188 model, respectively, and one and two 16-node cubic cross-sectional elements for the proposed warping beam model, respectively. The constrained boundary condition $u = v = $

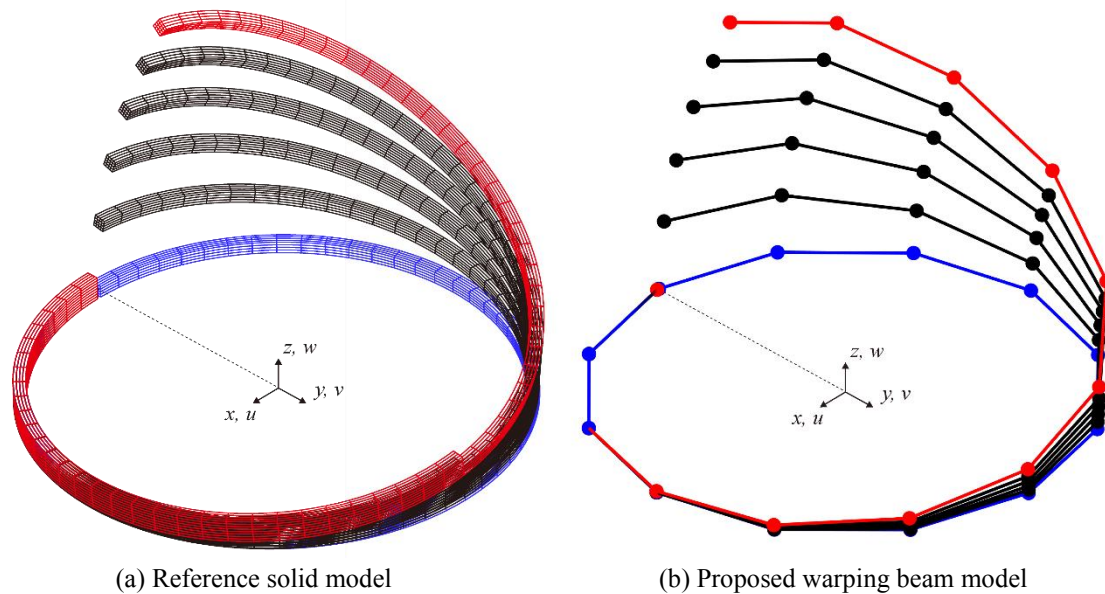(a) Reference solid model (b) Proposed warping beam model

Fig. 22 Deformed configurations of the circular beam with a step varying rectangular cross-section

$w = \theta_x = \theta_y = \theta_z = \alpha = 0$ and force $F_z = 1.5 \times 10^6 N$ are applied at $\phi = 0°$ and $\phi = 359°$, respectively.

Fig. 20 shows the load-displacement curves considering the displacements of point A at the free end. The results from the proposed warping beam model correspond well with those from the reference solid model. Fig. 21 presents the y and z-directional displacements (v and w) of point A according to the angle ϕ when $F_z = 1.5 \times 10^6$ N. These results confirm that the proposed interface warping function can be adopted to calculate complex beam problems considering twisting-bending coupling using only 7 DOFs per node. Fig. 22 shows the successive deformed configurations obtained using the reference solid model and the proposed warping beam model at various load levels ($F_z = 0.3 \times 10^6$ N, 0.6×10^6 N, 0.9×10^6 N, 1.2×10^6 N, and 1.5×10^6 N). The geometric nonlinear response due to twisting-bending coupling is accurately predicted using the proposed warping beam model.

5. Conclusions

In this paper, we proposed a numerical method that can effectively calculate interface warping functions for beams with geometrical and material discontinuities in the longitudinal direction. The governing equations were obtained by extending the classical Saint Venant torsion theory along the longitudinal direction. Finite element discretization was developed to numerically calculate the proposed interface warping functions and the corresponding twisting centers. The interface warping functions are incorporated with the continuum-mechanics based beam element. Consequently, a general 3D beam finite element capable of modeling longitudinal discontinuities was developed for linear and nonlinear analysis while using only 7 DOFs per node.

The proposed beam finite element can consider partially/fully constrained warping conditions, curved geometries, composite materials, longitudinal discontinuities in material and geometry, and arbitrary cross-sections. Through numerical examples, powerful modeling and predictive capabilities of the proposed warping beam model were demonstrated in both linear and geometric nonlinear analysis. An important advantage of the interface warping functions presented in this study is that the displacement compatibility at an interface cross-section can be satisfied using only 7 DOFs per node. The interface warping functions can be easily adopted to other types of beam finite elements, allowing consideration of material and geometric longitudinal discontinuities.

References

Alsafadie, R., Hjiaj, M. and Battini, J.M. (2011), "Three-dimensional formulation of a mixed corotational thin-walled beam element incorporating shear and warping deformation", *Thin Wall. Struct.*, **49**, 523-533. https://doi.org/10.1016/j.tws.2010.12.002.

ANSYS (2018), ANSYS Mechanical APDL Theory Reference, ANSYS Inc.

Barretta, R., Luciano, R. and Willis, J.R. (2015), "On torsion of random composite beams", *Compos. Struct.*, **132**, 915-922.

https://doi.org/10.1016/j.compstruct.2015.06.069.

Bathe, K.J. (1996), *Finite Element Procedures*, Prentice Hall, New York.

Batoz, J.L. and Dhatt, G. (1990), *Modélisation des Structures par Eléments Finis: Solides Elastiques*, Hermes Sciences.

Battini, J.M. and Pacoste, C. (2002), "Co-rotational beam elements with warping effects in instability problems", *Comput. Meth. Appl. Mech. Eng.*, **191**, 1755-1789. https://doi.org/10.1016/S0045-7825(01)00352-8.

Benscoter, S.U. (1954), "A theory of torsion bending for multicell beams", *J. Appl. Mech.*, **21**, 25-34. https://doi.org/10.1115/1.4010814.

Cardona, A. and Geradin, M. (1988), "A beam finite element non-linear theory with finite rotations", *Int. J. Numer. Meth. Eng.*, **26**, 2403-2438. https://doi.org/10.1002/nme.1620261105.

Carrera, E., Giunta, G., Nali, P. and Petrolo, M. (2010), "Refined beam elements with arbitrary cross-section geometries", *Comput. Struct.*, **88**, 283-293. https://doi.org/10.1016/j.compstruc.2009.11.002.

Dvorkin, E.N., Celentano, D., Cuitiño, A. and Gioia, G. (1989), "A Vlasov beam element", *Comput. Struct.*, **33**, 187-196. https://doi.org/10.1016/0045-7949(89)90140-5.

El Fatmi, R. (2007a), "Non-uniform warping including the effects of torsion and shear forces. Part I: A general beam theory", *Int. J. Solid. Struct.*, **44**, 5912-5929. https://doi.org/10.1016/j.ijsolstr.2007.02.006.

El Fatmi, R. (2007b), "Non-uniform warping including the effects of torsion and shear forces. Part II: Analytical and numerical applications", *Int. J. Solid. Struct.*, **44**, 5930-5952. https://doi.org/10.1016/j.ijsolstr.2007.02.005.

El Fatmi, R. and Ghazouani, N. (2011a), "Higher order composite beam theory built on Saint-Venant's solution. Part-I: Theoretical developments", *Compos. Struct.*, **93**, 557-566. https://doi.org/10.1016/j.compstruct.2010.08.024.

Genoese, A., Genoese, A., Bilotta, A. and Garcea, G. (2013), "A mixed beam model with non-uniform warpings derived from the Saint Venànt rod", *Comput. Struct.*, **121**, 87-98. https://doi.org/10.1016/j.compstruc.2013.03.017.

Genoese, A., Genoese, A., Bilotta, A. and Garcea, G. (2014), "A geometrically exact beam model with non-uniform warping coherently derived from the Saint Venant rod", *Eng. Struct.*, **68**, 33-46. https://doi.org/10.1016/j.engstruct.2014.02.024.

Ghazouani, N. and El Fatmi, R. (2011b), "Higher order composite beam theory built on Saint-Venant's solution. Part-II: Built-in effects influence on the behavior of end-loaded cantilever beams", *Compos. Struct.*, **93**, 567-581. https://doi.org/10.1016/j.compstruct.2010.08.024.

Gjelsvik, A. (1981), *The Theory of Thin Walled Bars*, Wiley, New York.

GonÇalves, R., Ritto-Corrêa, M. and Camotim, D. (2010), "A large displacement and finite rotation thin-walled beam formulation including cross-section deformation", *Comput. Meth. Appl. Mech. Eng.*, **199**, 1627-1643. https://doi.org/10.1016/j.cma.2010.01.006.

Gruttmann, F., Sauer, R. and Wagner, W. (1999), "Shear stresses in prismatic beams with arbitrary cross-sections", *Int. J. Numer. Meth. Eng.*, **45**, 865-889. https://doi.org/10.1002/(SICI)1097-0207(19990710)45:7<865::AID-NME609>3.0.CO;2-3.

Hughes, T.J.R. (2000), *The Finite Element Method: Linear Static and Dynamic Finite Element Analysis*, Dover Publications.

Ibrahimbegović, A. (1995), "On finite element implementation of geometrically nonlinear Reissner's beam theory: three-dimensional curved beam elements", *Comput. Meth. Appl. Mech. Eng.*, **122**, 11-26. https://doi.org/10.1016/0045-7825(95)00724-F.

Ibrahimbegovic, A. (1997), "On the choice of finite rotation parameters", *Comput. Meth. Appl. Mech. Eng.*, **149**, 49-71.

https://doi.org/10.1016/S0045-7825(97)00059-5.

Iesan, D. (2008), *Classical and Generalized Models of Elastic Rods*, Chapman and Hall/CRC, New York.

Kim, H.J., Lee, D.H., Yoon, K. and Lee, P.S. (2021), "A multi-director continuum beam finite element for efficient analysis of multi-layer strand cables", *Comput. Struct.*, **256**, 106621. https://doi.org/10.1016/j.compstruc.2021.106621.

Kim, H.J., Yoon, K. and Lee, P.S. (2020), "Continuum mechanics based beam elements for linear and nonlinear analyses of multi-layered composite beams with interlayer slips", *Compos. Struct.*, **235**, 111740. https://doi.org/10.1016/j.compstruct.2019.111740.

Lee, P.S. and McClure, G. (2006), "A general three-dimensional L-section beam finite element for elastoplastic large deformation analysis", *Comput. Struct.*, **84**, 215-229. https://doi.org/10.1016/j.compstruc.2005.09.013.

Mancusi, G. and Feo, L. (2013), "Non-linear pre-buckling behavior of shear deformable thin-walled composite beams with open cross-section", *Compos. B. Eng.*, **47**, 379-390. https://doi.org/10.1016/j.compositesb.2012.11.003.

Pacoste, C. and Eriksson, A. (1977), "Beam elements in instability problems", *Comput. Meth. Appl. Mech. Eng.*, **144**, 163-197. https://doi.org/10.1016/S0045-7825(96)01165-6.

Petrov, E. and Géradin, M. (1998a), "Finite element theory for curved and twisted beams based on exact solutions for three-dimensional solids. Part 1: Beam concept and geometrically exact nonlinear formulation", *Comput. Meth. Appl. Mech. Eng.*, **165**, 43-92. https://doi.org/10.1016/S0045-7825(98)00061-9.

Petrov, E. and Géradin, M. (1998b), "Finite element theory for curved and twisted beams based on exact solutions for three-dimensional solids. Part 2: Anisotropic and advanced beam models", *Comput. Meth. Appl. Mech. Eng.*, **165**, 93-127. https://doi.org/10.1016/S0045-7825(98)00060-7.

Pi, Y.L., Bradford, M.A. and Uy, B. (2005), "Nonlinear analysis of members curved in space with warping and Wagner effects", *Int. J. Solid. Struct.*, **42**, 3147-3169. https://doi.org/10.1016/j.ijsolstr.2004.10.012.

Qureshi, MAM. and Ganga Rao, H. (2014), "Torsional response of closed FRP composite sections", *Compos. B. Eng.*, **61**, 254-266. https://doi.org/10.1016/j.compositesb.2013.12.065

Sapountzakis, E.J. and Mokos, V.G. (2003), "Warping shear stresses in nonuniform torsion of composite bars by BEM", *Comput. Meth. Appl. Mech. Eng.*, **192**, 4337-4353. https://doi.org/10.1016/S0045-7825(03)00417-1.

Sapountzakis, E.J. and Mokos, V.G. (2004), "Nonuniform torsion of composite bars of variable thickness by BEM", *Int. J. Solid. Struct.*, **41**, 1753-1771. https://doi.org/10.1016/j.ijsolstr.2003.11.025.

Timoshenko, S.P. and Goodier, J.N. (1970), *Theory of Elasticity*, McGraw Hill.

Vlasov, V.Z. (1961), *Thin-walled Elastic Beams*, Israel Program for Scientific Translations, Jerusalem.

Wagner, W. and Gruttmann, F. (2001), "Finite element analysis of Saint-Venant torsion problem with exact integration of the elastic-plastic constitutive equations", *Comput. Meth. Appl. Mech. Eng.*, **190**, 3831-3848. https://doi.org/10.1016/S0045-7825(00)00302-9.

Wagner, W. and Gruttmann, F. (2002), "A displacement method for the analysis of flexural shear stresses in thin-walled isotropic composite beams", *Comput. Struct.*, **80**, 1843-1851. https://doi.org/10.1016/S0045-7949(02)00223-7.

Yoon, K. and Lee, P.S. (2014a), "Modeling the warping displacements for discontinuously varying arbitrary cross-section beams", *Comput. Struct.*, **131**, 56-69. https://doi.org/10.1016/j.compstruc.2013.10.013.

Yoon, K. and Lee, P.S. (2014b), "Nonlinear performance of continuum mechanics based beam elements focusing on large twisting behaviors", *Comput. Meth. Appl. Mech. Eng.*, **281**, 106-30. https://doi.org/10.1016/j.cma.2014.07.023.

Yoon, K., Kim, D.N. and Lee, P.S. (2017b), "Nonlinear torsional analysis of 3D composite beams using the extended St. Venant solution", *Struct. Eng. Mech.*, **62**, 33-42. https://doi.org/10.12989/sem.2017.62.1.033.

Yoon, K., Lee, P.S. and Kim, D.N. (2015), "Geometrically nonlinear finite element analysis of functionally graded 3D beams considering warping effects", *Compos. Struct.*, **132**, 1231-1247. https://doi.org/10.1016/j.compstruct.2015.07.024.

Yoon, K., Lee, P.S. and Kim, D.N. (2017a), "An efficient warping model for elastoplastic torsional analysis of composite beams", *Compos. Struct.*, **178**, 37-49. https://doi.org/10.1016/j.compstruct.2017.07.041.

Yoon, K., Lee, Y. and Lee, P.S. (2012), "A continuum mechanics based 3-D beam finite element with warping displacements and its modeling capabilities", *Struct. Eng. Mech.*, **43**, 411-437. https://doi.org/10.12989/sem.2012.43.4.411.

CC